



Research  
Carbon Neutrality Pathways for Building Operation—Review

## Excellent Insulation Vacuum Glazing for Low-Carbon Buildings: Fabrication, Modeling, and Evaluation



Jinqing Peng<sup>a,b,\*</sup>, Yutong Tan<sup>a,b,\*</sup>, Yueping Fang<sup>c</sup>, Hongxing Yang<sup>d</sup>, Aotian Song<sup>e</sup>, Charlie Curcija<sup>f</sup>, Stephen Selkowitz<sup>f</sup>

<sup>a</sup> College of Civil Engineering, Hunan University, Changsha 410082, China

<sup>b</sup> Key Laboratory of Building Safety and Energy Efficiency of the Ministry of Education, Changsha 410082, China

<sup>c</sup> School of Energy, Construction and Environment, Coventry University, Coventry CV1 5FB, UK

<sup>d</sup> Renewable Energy Research Group (RERG), Department of Building Environment and Energy Engineering, The Hong Kong Polytechnic University, Hong Kong 999077, China

<sup>e</sup> Leadus Glass Technology (Shenzhen) Co., Ltd., Shenzhen 518000, China

<sup>f</sup> Building Technology and Urban Systems Division, Lawrence Berkeley National Laboratory, Berkeley CA 94720, USA

### ARTICLE INFO

#### Article history:

Received 4 June 2024

Revised 3 October 2024

Accepted 29 November 2024

Available online 10 December 2024

#### Keywords:

Vacuum glazing

Fabrication approach

Thermal performance

Modeling method

Energy-savings potential

### ABSTRACT

Vacuum glazing is highly regarded for its ability to transmit light while providing heat preservation, sound insulation, lightweight characteristics, and resistance to condensation. Scholars have made significant strides in the study of vacuum glazing through their notable efforts. This study systematically reviewed vacuum glazing and its composite structures, including material selection, fabrication techniques, research methods, and performance evaluation. This review initially presented fundamental techniques for preparing vacuum glazing, with a focus on edge seal and support pillar arrangements, and introduced common composite structures such as hybrid and tinted vacuum glazing. Furthermore, this review summarized the analytical, numerical, and experimental methodologies used to assess the thermal performance of vacuum glazing. This study also outlined heat transfer coefficients associated with various vacuum glazing structures, investigated the influence of different parameters on their heat transfer coefficients, and evaluated their potential for energy conservation across diverse climatic regions. Finally, the research delineated future trends in the advancement of vacuum glazing to provide guidance for both theoretical studies and practical applications in industry. This research serves as a valuable resource for both theoretical exploration and practical integration of vacuum glazing, facilitating its improvement and optimization to advance sustainable low-carbon building practices.

© 2024 THE AUTHORS. Published by Elsevier LTD on behalf of Chinese Academy of Engineering and Higher Education Press Limited Company. This is an open access article under the CC BY-NC-ND license (<http://creativecommons.org/licenses/by-nc-nd/4.0/>).

## 1. Introduction

### 1.1. Research background

Commercial and residential buildings account for approximately 40% of society's total energy consumption [1,2] and are utilized primarily to maintain the desired thermal and daylight indoor environment. The building envelopes, especially transparent glazing, serve as the boundary between the external natural world and the internal artificial environment, exerting a significant effect on the indoor environment [3]. Owing to the poor thermal

insulating properties of conventional glazing, a considerable portion of building energy is lost [4,5]. Therefore, the advancement of energy-efficient glazing is paramount for realizing low-carbon buildings.

To improve the thermal performance of glazing in buildings, researchers have developed multicavity low-efficiency glazing filled with inert gases [6–8], vacuum glazing [9,10], and aerogel glazing [11,12]. The frequency-selective surface technique was applied to low-emissivity (low-E) windows to address the problem of telecommunication signal attenuation caused by metal layers [13]. By filling the cavity with argon instead of air, the heat transfer coefficient ( $U$ -value) of double-pane glazing can be reduced from 2.70 to 1.80  $W \cdot m^{-2} \cdot K^{-1}$  [14]. Furthermore, it can be improved by using two low-E coatings and two argon cavities, resulting in a  $U$ -value of 0.79  $W \cdot m^{-2} \cdot K^{-1}$  [15]. Nevertheless, the accompanying

\* Corresponding authors.

E-mail addresses: [jqpeng@hnu.edu.cn](mailto:jqpeng@hnu.edu.cn) (J. Peng), [sharontyt@hnu.edu.cn](mailto:sharontyt@hnu.edu.cn) (Y. Tan).

problems of increased thickness and weight limit its application in existing buildings [16]. Vacuum glazing can effectively solve these problems, reducing the  $U$ -value below  $1.0 \text{ W}\cdot\text{m}^{-2}\cdot\text{K}^{-1}$  without increasing the thickness [17]. Similarly, aerogel glazing can achieve this effect, with a central  $U$ -value of  $0.21 \text{ W}\cdot\text{m}^{-2}\cdot\text{K}^{-1}$  [18]. However, aerogel glazing has not been industrialized and applied on a large scale because of its weak mechanical properties and high degree of fogging [19]. Therefore, this study focused on vacuum glazing and was devoted to conducting a thorough review of the fabrication, simulation, and evaluation of glazing.

### 1.2. Timeline of vacuum glazing advancements

The evolution of vacuum glazing technology is depicted in Fig. 1. The idea of vacuum glazing was initially outlined in 1913 [20]. A series of support pillars was set within the vacuum gap to withstand the external pressure and maintain separation between two glass sheets [21]. After extensive research and development, the first vacuum glazing sample was reported in 1985, but its thermal performance was compromised by inadequate vacuum pressure [22]. In 1989, employing glass solder sealing technology, researchers at the University of Sydney, Australia, successfully produced vacuum glazing with excellent thermal insulation performance [23]. Subsequently, Collins and Simko [24] summarized the methods of fabricating vacuum glazing. The Nippon Sheet Glass (NSG) Group, Japan, attempted to commercialize this vacuum glazing in the 2000s in collaboration with the University of Sydney, Australia, the  $U$ -value of which is approximately  $1.5 \text{ W}\cdot\text{m}^{-2}\cdot\text{K}^{-1}$  [25]. However, the high sealing temperature poses a challenge for the application of tempered glass and low-E coatings in vacuum glazing because of their characteristic degradation. To address this, researchers at Ulster University, UK, developed a different sealing technique with a low melting temperature of approximately  $150 \text{ }^\circ\text{C}$  and an indium alloy as the sealing material [26,27]. On the basis of these two different fabrication methods, researchers have developed various vacuum glazing samples and have conducted extensive studies on their thermal properties. In 2018, the WINDOW and THERM software packages incorporated a thermal performance module for vacuum glazing created by researchers at Lawrence Berkeley National Laboratory, USA [28]. Researchers subsequently carried out related studies on the energy savings potential of vacuum glazing by combining WINDOW and Energy-Plus softwares (USA).

This study conducted a search with the Web of Science search engine using keywords such as “vacuum glazing,” “vacuum window,” “evacuated glazing,” or “evacuated window” from 2003 to 2023, resulting in a total of 159 publications, as depicted in Fig. 2. A literature source analysis revealed that 83 publications

were from Asia, 63 from Europe, 8 from North America, and 5 from Oceania. In terms of distribution by nation, Chinese researchers provided the most literature during this period, accounting for 33.3% of the total publications, followed by the United Kingdom (UK) and Republic of Korea, which contributed 22.6% and 11.9%, respectively.

In a summary of 159 studies, as shown in Fig. 3., 62.8% of the studies pertain to vacuum glazing systems, whereas 37.2% focus on composite vacuum glazing systems. Among the latter category, composite vacuum glazing includes various types, such as photovoltaic (PV) vacuum glazing, multilayer vacuum glazing, tinted vacuum glazing, and water flow, aerogel, and phase change material (PCM) vacuum glazing, which account for 40%, 33%, 17%, 6%, 2%, and 2% of composite vacuum glazing systems, respectively. Among the studies on different types of vacuum glazing, 39.3% have focused on their thermal properties, and 33.1% have delved into their comprehensive properties. Additionally, studies on the preparation process, stress analysis, and optical properties of vacuum glazing account for 15.2%, 9.7%, and 2.8%, respectively.

### 1.3. Motivation and objectives

In the past two decades, four review articles have been published on vacuum glazing, covering topics such as its thermal performance [29,30], the design aspects of multi-vacuum glazing [31], and the performance evaluation of PV vacuum glazing [32]. Considering the energy crisis and climate change, many scholars and enterprises hold a positive outlook for the future advancement of vacuum glazing in buildings. However, a thorough and systematic summary of vacuum glazing systems, including their preparation technology, material selection, research methodologies, and performance analysis, is lacking. Therefore, the primary goal of this research is to provide a comprehensive systematic review of the fabrication methods, heat transfer processes, research methods, and energy savings potential of vacuum glazing. First, an overview of the fabrication technology and common materials used in vacuum glazing was provided. This is followed by a discussion of novel composite vacuum glazing structures derived from traditional double-pane vacuum glazing, along with an analysis of their respective advantages and disadvantages. Various analytical, numerical, and experimental methods for assessing the thermal performance of vacuum glazing were subsequently outlined. Through a comprehensive literature review, the  $U$ -values of different typical vacuum glazing structures were presented and compared, alongside a summary of the impacts of various factors on the thermal performance of vacuum glazing. Finally, the energy performance of different types of vacuum glazing in diverse climates was explored, and the regional suitability of different

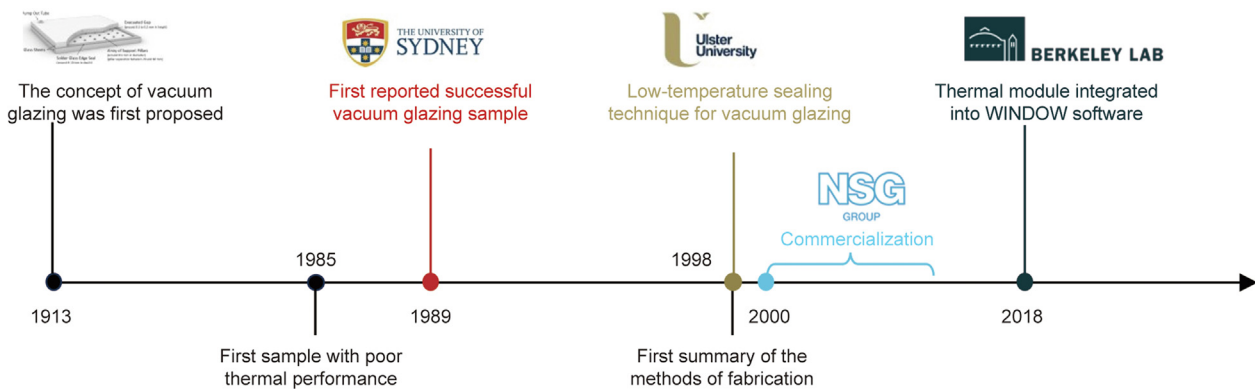


Fig. 1. Development history diagram of vacuum glazing.

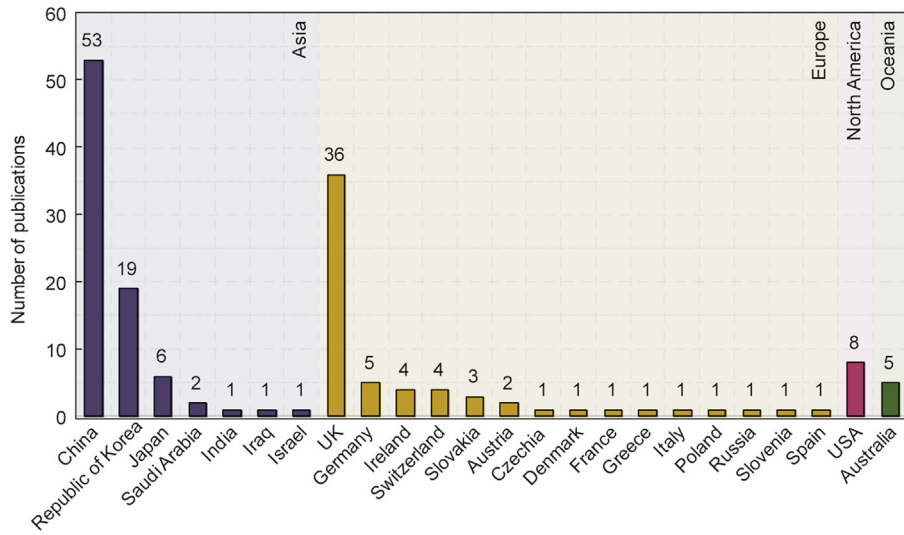


Fig. 2. Publications distribution on vacuum glazing around the world in the past two decades.

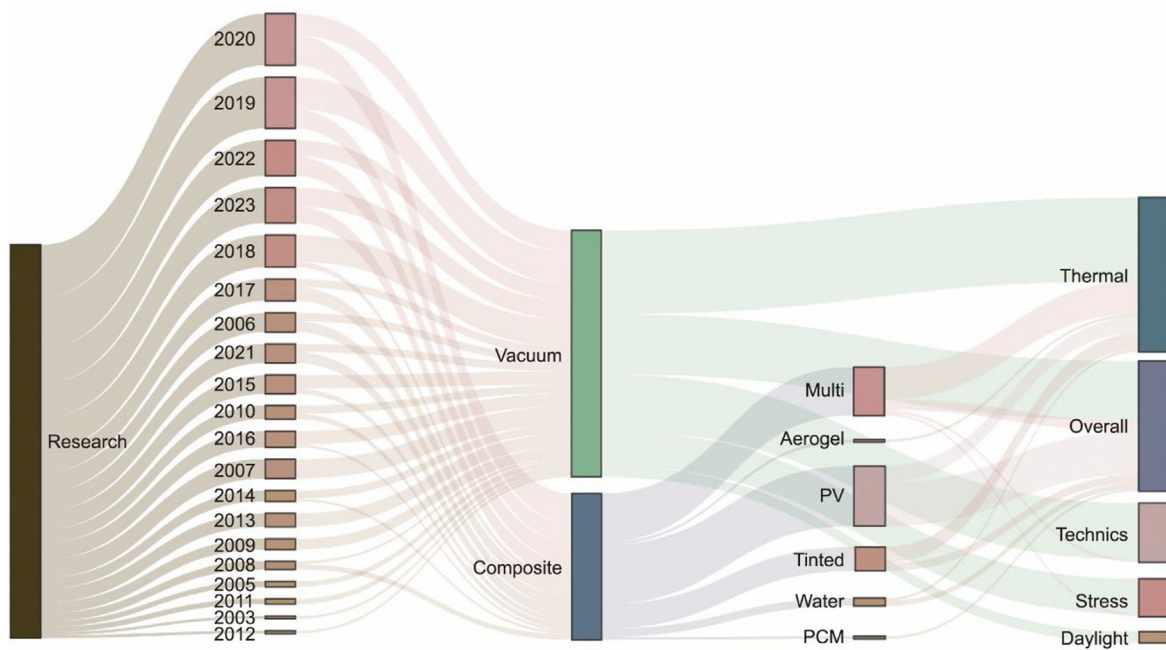


Fig. 3. Research objects and focused performance. “Vacuum” refers to conventional double-pane vacuum glazing, “Composite” refers to vacuum glazing composited with other technologies, like multi-pane vacuum glazing (Multi), aerogel-vacuum glazing (Aerogel), PV-vacuum glazing (PV), tinted-vacuum glazing (Tinted), water flow vacuum glazing (Water), and PCM-vacuum glazing (PCM). The performance studied include thermal performance (Thermal), overall performance (Overall), preparation techniques (Technics), stress performance (Stress) and daylight performance (Daylight).

vacuum glazing structures was analyzed. The systematic review presented in this paper provides valuable guidance for theoretical research, optimal design, and industrial development in vacuum glazing.

## 2. Fabrication methods and products

### 2.1. Fabrication processes with different sealing techniques

Currently, there are three main fabrication methods for vacuum glazing: the solder glass (SG) edge sealing method, the vacuum chamber (VC) edge sealing method, and the pump-out (PO) edge sealing method [33,34]. The details of the above three methods are shown in Fig. 4. For all methods, the first step is to clip the glass

pane to the required size. To connect the PO tube for the SG method and PO method, a tiny hole must be drilled in the upper glass corner. Then, the glass sheets are cleaned with acetone and deionized water and dried. Following these steps, a series of support pillars are placed on the bottom glass pane with appropriate spacing. Before the upper glass cover is placed, sealing material (glass powder or indium alloy) is applied around the glass sheets. For the SG method, the entire assembly is subsequently placed in an oven at 450 °C to create a hermetic seal surrounding the perimeter. Once the glazing is cooled to room temperature, the evacuation process begins, accompanied by a bake-out process from 100 to 250 °C to outgas the interior surfaces. When the glazing is cooled to room temperature again, a tungsten coil is used to melt and seal the PO tube, and the vacuum glazing process is

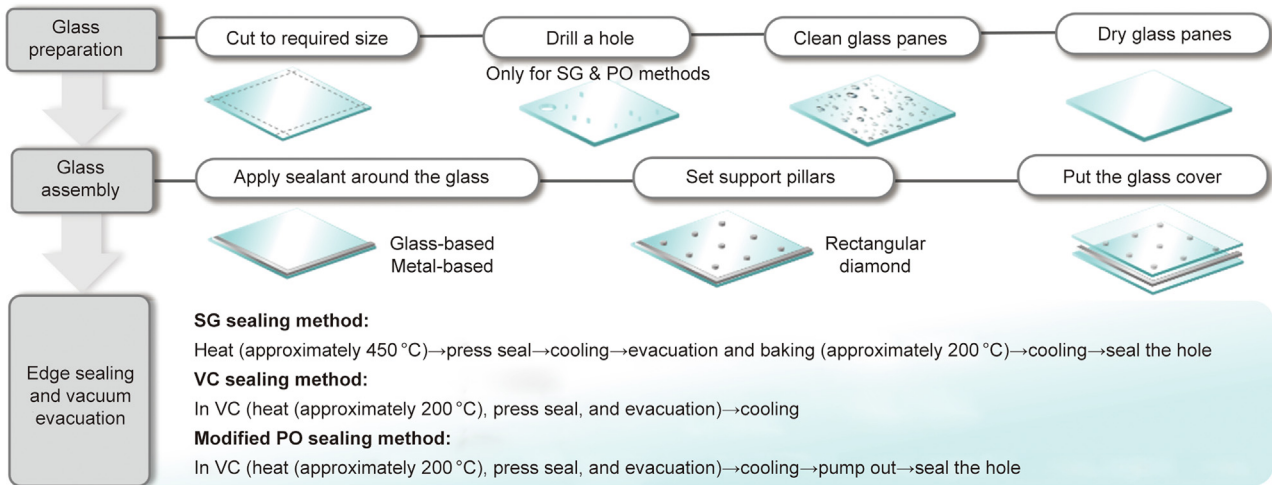


Fig. 4. Detailed steps of three vacuum glazing fabrication methods.

complete. Unlike the SG method, in the VC and PO methods, the sealing and evacuation processes are carried out simultaneously in a VC with a vacuum of approximately  $10^{-5}$  Pa. The VC is initially heated to approximately 150 °C to facilitate outgassing and then further increased to 170 °C to fuse the indium alloys. The heating and vacuum pump systems are subsequently turned off, and the VC method is finished. For the PO method, the heating system is first turned off, and the assembly is allowed to cool to room temperature. Then, a pump system is engaged to form the desired vacuum. Finally, the PO hole is sealed, and sample preparation is completed.

On the basis of the above analysis, the distinction in fabrication methods lies primarily in the sealing temperature, with the sealing material dictating this parameter. Among these materials, glass solder sealing materials have a thermal expansion coefficient similar to that of glass sheets, which mitigates potential glass damage caused by thermal stress [29]. However, it requires a high melting temperature, which may lead to the degradation of tempered glass and the failure of low-E coatings [27,29]. The alloy solder boasts a lower melting temperature but inadequate long-term resistance to moisture penetration [26,35], requiring a more demanding pumping process and equipment. In addition to these materials, researchers are actively exploring the development of new sealants and technologies [36,37]. As the main component for preventing vacuum glazing failure, the sealing material must satisfy several criteria: ① a low melting temperature to mitigate issues such as stress decay in tempered glass and failure of low-E films; ② a thermal expansion coefficient compatible with that of glass; and ③ high stability to prevent significant performance deterioration over extended service periods.

### 2.2. Support pillar arrangement and materials

In addition to sealing technology, the arrangement of the support array within the VC is crucial for successful fabrication. To ensure separation between the two glass panes, a support pillar array must be positioned to counteract the external atmospheric pressure. The configuration of support pillars must balance both mechanical and thermal considerations: A sparse support array risks glass breakage, whereas excessive density exacerbates the thermal bridge effect. For the trade-off between mechanical and thermal performance, several design principles for the support pillar array are outlined [38,39]:

The spacing between pillars has a maximum limit due to the constraint of tensile stress [40]:

$$0.11 \frac{\lambda^2}{t^2} \leq t_s \tag{1}$$

where  $t_s$  is the tensile stress limit of the glass sheets:  $t_s = 4$  Mpa for annealed glass;  $t_s = 35$  Mpa for tempered glass.  $\lambda$  is the spacing, m;  $t$  is the thickness of the glass sheet, mm.

The compressive strength requirements of support pillars can be written as follows [41]:

$$\frac{q\lambda^2}{\pi a^2} \leq c_s \tag{2}$$

where  $q$  is the atmospheric pressure, MPa;  $a$  is the radius of support pillars, m;  $c_s$  is the compressive stress limit of the support pillar material, MPa.

Hertzian conical fractures are avoided because of the contact pressure limit [38,42]:

$$\lambda < \frac{(\frac{4AE}{3})^{\frac{1}{4}} a^{\frac{3}{4}}}{\sqrt{q}} \tag{3}$$

where  $A$  is the Auerbach constant, with  $A = 10^5 \text{ N} \cdot \text{M}^{-1}$ ;  $E$  is the Young's modulus, MPa.

The Euler buckling risk is avoided [43]:

$$a \geq \left( \frac{2q\lambda^2 h^2}{\pi^2 E} \right)^{\frac{1}{4}} \tag{4}$$

where  $h$  is the height of the support pillar, mm.

The thermal conductance constraint is as follows [44]:

$$\frac{2k_g a}{\lambda^2} < A_{\min} \tag{5}$$

where  $k_g$  is the thermal conductivity of the glass pane,  $\text{W} \cdot \text{m}^{-1} \cdot \text{K}^{-1}$ , and  $A_{\min}$  is the minimum heat transfer of the support pillars.

The parameters of commonly used vacuum glazing materials, such as their thermal conductivity and Young's modulus, are summarized in Table 1. By integrating all the above principles, as shown in Fig. 5 [45], the design parameters of the support pillars—specifically, the radius, spacing, and height—were selected.

### 2.3. Composite vacuum glazing

With significant efforts from researchers and manufacturers, the thermal performance of conventional vacuum glazing is approaching theoretical limits. Consequently, scholars have pro-

**Table 1**  
Summary of support pillar materials' properties.

Material	Conductivity ( $\text{W}\cdot\text{m}^{-1}\cdot\text{K}^{-1}$ )	Young's module (MPa)	Compressive stress (MPa)
Stainless steel	15.2	184 000	1 040
Aluminium alloy	201.0	70 000	500
Glass	1.0	55 000	60
Ceramic	1.1	300 000	60
Aerogel	0.024	113	167

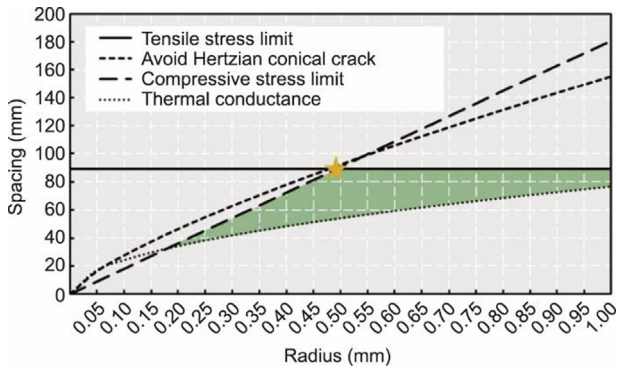


**Fig. 5.** Schematic diagram of the design for an array of support pillars. Reproduced from Ref. [45] with permission.

posed several composite vacuum glazing techniques, including multicavity, tinted, and PV vacuum glazing, as depicted in Fig. 6. Multicavity vacuum glazing refers to glazing that incorporates more than one cavity. Building upon the single vacuum glazing technique, hybrid vacuum glazing [46,47] and triple vacuum glazing [48] have been proposed. Hybrid vacuum glazing involves a vacuum layer and an insulating layer filled with inert gas such as argon, krypton, xenon, and others. Triple vacuum glazing involves three glass sheets and two vacuum gaps. In addition to improving the solar modulation ability of vacuum glazing, scholars have integrated vacuum glazing with dynamic technologies capable of responding to outdoor environments and occupant requirements, including suspended particle devices (SPDs) [49,50], liquid crystals (LCs) [51,52], and electrochromic (EC) [53,54] technologies. When no voltage is applied, both the SPD and the LC are in a tinted state. However, upon voltage application, internal randomly oriented microscopic particles and LC droplets align in parallel, allowing light transmission. SPD glazing and LC glazing have two drawbacks: ① They require continuous energy input to sustain the clear state, and ② they offer only clear and fully tinted states. EC glazing is an active solar control device whose transmittance can be rever-

sibly modulated by applying a switching voltage [55]. By integrating dynamic technologies, composite vacuum glazing can not only reduce heating loads but also mitigate cooling loads by modulating excessive solar radiation heat within rooms, leading to further reductions in building loads [56,57]. Researchers subsequently proposed combining vacuum glazing with solar cells to achieve net-zero energy buildings [45,58]. The PV layer typically faces the outdoor environment to capture incident solar radiation, whereas the vacuum glazing layer is oriented toward the indoor environment to minimize heat loss. The advantages and disadvantages of these composite vacuum glazing are summarized and listed in Table 2. In addition to these composite structures, researchers have suggested water flow vacuum glazing [59,60], aerogel vacuum glazing [61], and phase change vacuum glazing [62,63], but their safety and industrialization potential are somewhat limited. Therefore, these three composite structures were excluded from the subsequent performance analysis.

**2.4. Industrialization development of vacuum glazing**

With the development of vacuum glazing fabrication technologies, many companies worldwide have successfully industrialized vacuum glazing. The first commercially available vacuum glazing in the world, Spacia™, was launched by Nippon Sheet Glass (NSG) Co., Ltd., Japan [64]. The  $U$ -value of Spacia™ glazing is approximately  $1.10 \text{ W}\cdot\text{m}^{-2}\cdot\text{K}^{-1}$ , with a thickness of 6.2 mm. Another Japanese company, Asahi Glass Co., Ltd., partnered with Panasonic Ltd., Japan, to introduce Fineo™ vacuum glazing and hybrid vacuum glazing [65,66]. Fineo™ vacuum glazing, with a thickness of 7.7 mm, achieves a  $U$ -value of  $0.70 \text{ W}\cdot\text{m}^{-2}\cdot\text{K}^{-1}$ . Additionally, Fineo™ hybrid vacuum glazing, which consists of Fineo™ vacuum glazing, an argon gas cavity, and a low-E glass sheet, has a lower heat transfer coefficient of  $0.50 \text{ W}\cdot\text{m}^{-2}\cdot\text{K}^{-1}$ . Moreover, Vitro Architectural Glass, the largest glass manufacturer in Mexico, partnered with LandGlass Technology Co., Ltd. and VIG Technologies LLC., China, and launched a vacuum glazing product, VacuMax™ [67]. Other innovative products, called Enthermal™ and Enthermal Plus™, are produced by Luxwall, Inc., in Michigan [68]. In addition, four Chinese companies have commercialized and sold vacuum glazing on the market, namely, Synergy Energy Saving Glass (Tian jin) Co., Ltd. [69], Luoyang LandGlass Technologies Co., Ltd. [70], Henan Longwang Tempered Vacuum Glass Ltd. (ICESUN Vacuum Glass Ltd.), [71] and Shenzhen Leadus Technology Industry Co., Ltd. [72]. These companies abovementioned have introduced not only conventional double-pane vacuum glazing but also hybrid vacuum glazing. Shenzhen Leadus Technology Industry Co., Ltd., recently developed PV vacuum glazing. However, few companies have industrialized EC vacuum glazing, likely due to the high cost of EC technologies. Detailed information of these products, such as thickness,  $U$ -value, visible transmittance ( $T_{vis}$ ), and solar heat gain coefficient (SHGC), is listed in Table 3.

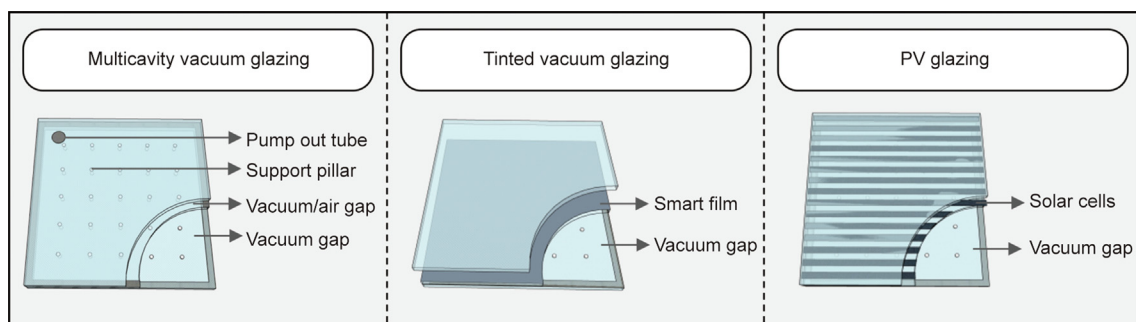


**Fig. 6.** Structure diagram of mainstream composite vacuum glazing.

**Table 2**  
Pros and cons of different vacuum glazing.

Glazing type	Subtype	Advantages	Disadvantages
Double-pane vacuum	–	Mature production technology Commercialized	The insulation performance is close to the theoretical limit
Multi-cavity vacuum	Triple	Excellent insulation performance	Difficult to produce
Tinted-vacuum	Hybrid	Low cost	Large thickness
	EC	Multiple available tinted states	Long response time
	SPD	Rapid state switching	High driving voltage (110 V)
PV-vacuum	LC	Rapid state switching	High driving voltage (20 V)
	–	Harness solar radiation to generate clean electricity	Reduce window penetration Affects occupants' vision

**Table 3**  
Detailed properties of commercialized vacuum products.

Institution	Product	Type	Thickness (mm)	U-value (W·m <sup>-2</sup> ·K <sup>-1</sup> )	T <sub>vis</sub>	SHGC	Sound insulation (dB)
NSG/Pilkington	Spacia™	Vacuum	6.2	1.10	0.78	0.67	–
Asahi Glass Co., Ltd.	Fineo™	Vacuum	7.7	0.70	0.80	0.62	30
		Hybrid vacuum	25.7	0.50	0.66	0.43	35
Vitro Architectural Glass Luxwall, Inc.	VacuMax™	Vacuum	8.3	0.30	0.62	0.25	–
		Hybrid vacuum	25.0	0.28	0.44	0.22	35
SynergyEnergy Saving Glass (Tianjin) Co., Ltd.	SYNERGY™	Vacuum	10.3	0.40	0.71	0.42	39
		Hybrid vacuum	27.3	0.37	0.64	0.39	40
Luoyang LandGlass Technologies Co., Ltd.	LandVac™	Vacuum	10.3	0.45	0.70	0.39	39
		Hybrid vacuum	27.3	0.44	0.62	0.37	41
ICESUN Vacuum Glass Ltd.	ICESUN™	Vacuum	10.2	0.50	0.62	–	41
		Hybrid vacuum	20.2	0.32	0.53	–	41
Shenzhen Leadus Technology Industry Co., Ltd.	–	Vacuum	10.2	≤ 0.30	0.63	0.31	> 40
		Hybrid vacuum	27.0	≤ 0.40	0.63	0.31	> 40
		PV-vacuum	–	≤ 0.50	0.60	–	> 40

### 3. Research methods and analysis of thermal performance

The most prominent advantage of vacuum glazing lies in its exceptional insulation performance, typically assessed through the *U*-value [73]. The *U*-value is further divided into the central *U*-value and total *U*-value [74,75]. This section outlines the analytical, numerical, and experimental methods for assessing the thermal performance of various vacuum structures. The effects of various factors on the *U*-value of vacuum glazing were subsequently summarized.

#### 3.1. Analytical research

The one-dimensional thermal resistance network approach, also known as the analytical method, is the most common method. Fig. 7 depicts the thermal resistance network of conventional double-pane vacuum glazing corresponding to a certain outdoor (*T*<sub>out</sub>) and indoor (*T*<sub>in</sub>) temperatures. The overall thermal resistance can be divided into three parts: ① the thermal resistance from the outermost surface of the vacuum glazing (*S*<sub>1</sub>) to the outdoor environment, *R*<sub>out</sub>, and from the innermost surface of the vacuum glazing (*S*<sub>4</sub>) to the indoor environment, *R*<sub>in</sub>; ② the heat conduction resistance of glass sheets (*R*<sub>g</sub>); and ③ the thermal conductivity and radiant resistance in the vacuum gap (*R*<sub>gap</sub>). Specifically, *R*<sub>gap</sub> consists of the radiative thermal resistance on two parallel surfaces (*S*<sub>2</sub> and *S*<sub>3</sub>) of the VC (*R*<sub>rad</sub>), the conductivity thermal resistance of the support pillar array (*R*<sub>pa</sub>), the residual gas (*R*<sub>gas</sub>), and the seal edge (*R*<sub>edge</sub>). Usually, heat transfer analysis of vacuum glazing is conducted on the basis of the following hypotheses and simplifications [76]:

- (1) The influence of different heat transfer modes is ignored.
- (2) The effects of different heat transfer modes on the thermal insulation performance can be superimposed.

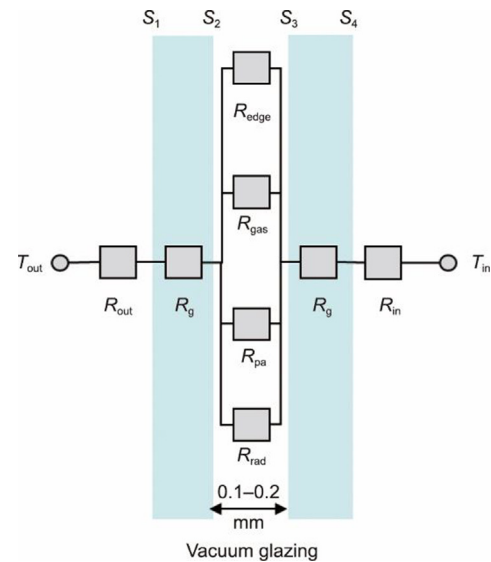


**Fig. 7.** Schematic diagram of vacuum glazing's thermal resistance network.

(3) The impact of the lateral surfaces of the support pillars on radiative heat transfer is considered negligible.

With the aforementioned hypotheses and simplifications, the central (*U*<sub>c</sub>) and total *U*-values (*U*<sub>tot</sub>) of vacuum glazing can be expressed [77]:

$$U_c = \frac{1}{R_{out} + 2R_g + R_{gap} + R_{in}} \tag{6}$$

$$R_{gap} = \frac{1}{R_{rad}^{-1} + R_{pa}^{-1} + R_{gas}^{-1}} \tag{7}$$

$$U_{tot} = \frac{Q_{total}}{A_{total}(T_{in} - T_{out})} \quad (8)$$

where  $Q_{total}$  is the total heat flow through the vacuum glazing, W and  $A_{total}$  is the area of the vacuum glazing, m<sup>2</sup>.

### 3.1.1. Thermal resistance of outdoor and indoor heat transfer

The outermost and innermost surfaces of vacuum glazing undergo mixed heat transfer via convection and radiation with outdoor and indoor environments. The mathematical description of the outdoor heat transfer coefficient ( $h_o$ ) is expressed in Eqs. (9)–(12) [78]:

$$h_o = h_{co} + h_{ro} \quad (9)$$

$$h_{co} = 5.62 + 3.9v_o \quad (10)$$

$$h_{ro} = \frac{\sigma \varepsilon_o (T_{sky}^2 + T_{s1}^2)(T_{sky}^2 - T_{s1}^2)}{T_{out} - T_{s1}} \quad (11)$$

$$T_{sky} = 0.552T_{out}^{1.5} \quad (12)$$

where  $h_{co}$  represents the outdoor convective heat transfer coefficient, W·m<sup>-2</sup>·K<sup>-1</sup>;  $h_{ro}$  represents the radiative heat transfer coefficient, W·m<sup>-2</sup>·K<sup>-1</sup>;  $v_o$  represents the outdoor wind velocity, m·s<sup>-1</sup>;  $\sigma$  represents the Stefan–Boltzmann constant ( $\sigma = 5.67 \times 10^{-8}$  W·m<sup>-2</sup>·K<sup>-4</sup>);  $\varepsilon_o$  represents the emissivity of the outermost surface of the glazing;  $T_{sky}$  represents the sky temperature, Kelvin (K); and  $T_{s1}$  represents the temperature of the outermost surface, K.

The mathematical expression of the indoor heat transfer coefficient ( $h_i$ ) is as follows [79]:

$$h_i = h_{ci} + h_{ri} \quad (13)$$

$$h_{ci} = 5.34 + 3.27v_i \quad (14)$$

$$h_{ri} = \sigma \varepsilon_i (T_{in}^2 + T_{s4}^2)(T_{in} + T_{s4}) \quad (15)$$

where  $h_{ci}$  and  $h_{ri}$  are the indoor convective and radiative heat transfer coefficients, W·m<sup>-2</sup>·K<sup>-1</sup>;  $v_i$  is the interior wind velocity, m·s<sup>-1</sup>;  $\varepsilon_i$  is the emissivity of the innermost surface; and  $T_{s4}$  is the temperature of the innermost surface, K. The typical standard conditions for calculating the  $U$ -value are summarized and listed in Table 4.

### 3.1.2. Thermal resistance of glass panes

The thermal resistance per unit area of the glass sheet is calculated via Eq. (16):

$$R_g = \frac{t_g}{A_g k_g} \quad (16)$$

where  $t_g$  is the glass thickness, m;  $A_g$  is the glass area, m<sup>2</sup>; and  $k_g$  is the glass thermal conductivity, W·m<sup>-1</sup>·K<sup>-1</sup>.

### 3.1.3. Thermal resistance of the vacuum layer

(1) **Radiative thermal resistance in the VC.** The low-E coating is transparent to daylight but reflects thermal radiation, acting as a radiation filter [31]. The radiative thermal resistance between two

parallel surfaces in a VC can be calculated via the following formulas:

$$R_{rad} = \left( \varepsilon_e \cdot \sigma \cdot \frac{T_{s2}^4 - T_{s3}^4}{T_{s2} - T_{s3}} \right)^{-1} \quad (17)$$

$$\frac{1}{\varepsilon_e} = \frac{1}{\varepsilon_2} + \frac{1}{\varepsilon_3} - 1 \quad (18)$$

where  $\varepsilon_e$  is the effective emissivity;  $\varepsilon_2$  and  $\varepsilon_3$  are the emissivities of the second and third surfaces within the VC; and  $T_{s2}$  and  $T_{s3}$  are the temperatures of the second and third surfaces within the vacuum, K.

(2) **Thermal resistance of the support pillar.** The thermal resistance of an individual support pillar comprises both its thermal conduction resistance and the contact thermal resistance with the glass surface. Typically, within a VC, the support pillar only contacts the glass, with a spacing of approximately 30 mm. In this scenario, the contact thermal resistance is calculated via the single-point contact model proposed by Cooper et al. [85]:

$$R_{pillar,contact} = \frac{1}{2k_g a} \quad (19)$$

where  $R_{pillar,contact}$  is the contact thermal resistance of a support pillar, m<sup>2</sup>·K·W<sup>-1</sup>.

For a single support pillar, the conduction thermal resistance is expressed as

$$R_{pillar,conduction} = \frac{h}{k_p \cdot \pi a^2} \quad (20)$$

where  $R_{pillar,conduction}$  is the conduction thermal resistance of a single support pillar, m<sup>2</sup>·K·W<sup>-1</sup>,  $h$  is the height of the pillar, m, and  $k_p$  is the material thermal conductivity of the support pillar, W·m<sup>-1</sup>·K<sup>-1</sup>.

Therefore, the thermal resistance of a single support pillar and the pillar array with a spacing of  $\lambda$  can be calculated via Eqs. (21) and (22) [86]:

$$R_{pillar} = \frac{1}{2k_g a} + \frac{h}{k_p \cdot \pi a^2} \quad (21)$$

$$R_{pa} = \frac{\lambda^2 \left( 1 + \frac{2k_g h}{k_p \pi a} \right)}{2k_g a} \quad (22)$$

where  $R_{pillar}$  is the thermal resistance of a single support pillar, m<sup>2</sup>·K·W<sup>-1</sup>.

(3) **Thermal resistance of residual gas.** While vacuum glazing contains the word “vacuum,” its interior is not a true vacuum. Typically, two glass panels are prepared in an environment with a vacuum level of 10<sup>-4</sup> Pa, yet the internal vacuum of the prepared vacuum glazing is usually approximately 10<sup>-3</sup> or 10<sup>-2</sup> Pa. In practice, the vacuum level within a chamber gradually increases due to environmental factors such as the air temperature, solar radiation, and wind velocity, potentially reaching atmospheric pressure.

**Table 4**  
Summary of commonly standard conditions for  $U$ -value calculation.

Standard	Typical standard condition $T_{in}$ (°C)	$T_{out}$ (°C)	$h_o$ (W·m <sup>-2</sup> ·K <sup>-1</sup> )	$h_i$ (W·m <sup>-2</sup> ·K <sup>-1</sup> )
ASTM C1363 [80]	21.1	-17.8	30	8.3
ISO 10077 [81]	20.0	0	25	7.7
KS F 2278 [82]	20.0	0	20	9.1
JGJ/T 151 [83]	20.0	-20.0	16	3.6
GB/T 22476 [84]	20.0	0	23	8.0

Therefore, this section explores the impact of various gas flow patterns on the thermal resistance of a VC. Additionally, a comprehensive gas heat transfer model is developed to accommodate its entire lifecycle.

According to kinetic molecular theory, the residual gas heat transfer process is affected by the type of gas, vacuum level, surface characteristics of the solid materials, and spatial dimensions. In addition, the heat transfer mechanisms of gases at different vacuum levels exhibit distinct behaviors. The Knudsen number ( $K_n$ ), which is the ratio of the mean free path ( $l$ ) of the gas molecules to the characteristic size of the molecular motion space, is typically used to determine the rarefaction of the gas. In vacuum glazing, the characteristic size is the thickness of the vacuum gap. When  $K_n \leq 1/100$ , the gas flow is viscous flow, with heat exchange occurring mainly between gas molecules; when  $1/100 < K_n \leq 1/3$ , the gas flow is considered to be Knudsen flow; and when  $K_n > 1/3$ , the gas flow is molecular flow. At this time, collisions between gas molecules can be ignored, and only interactions between gas molecules and the interface are considered [87]. The Knudsen number is calculated on the basis of the mean molecular free path, as expressed below:

$$l = \frac{kT}{\sqrt{2}\pi d^2 P} \quad (23)$$

where  $k$  is the Boltzmann constant,  $k = 1.381 \times 10^{-23} \text{ J} \cdot \text{K}^{-1}$ ;  $T$  is the temperature, K;  $d$  is the diameter of the gas molecule, m; and  $P$  is the pressure of the VC, Pa.

For viscous flow, the heat transfer process of residual gas follows Fourier's law [88]:

$$Q = \frac{K_{\text{gas}} \cdot A_g (T_{s2} - T_{s1})}{L} \quad (24)$$

where  $Q$  is the heat flow per length of the vacuum gap, W;  $K_{\text{gas}}$  is the conductivity of the residual gas,  $\text{W} \cdot \text{m}^{-1} \cdot \text{K}^{-1}$ , and  $L$  is the thickness of the vacuum gap, m.

In Knudsen flow, molecular collisions are limited, resulting in heat transfer, primarily through interactions between molecules and the surface. However, the exchange of collision energy between molecules and the surface is insufficient, preventing gas molecules from reaching the surface temperature postcollision. Consequently, a temperature jump occurs between gas molecules and the surface, allowing for heat transfer calculations via the following formula:

$$Q = K_{\text{gas}} \frac{T_{s2} - T_{s1}}{L + 2g} A_g \quad (25)$$

$$g = l \frac{2 - \vartheta}{\vartheta} \quad (26)$$

$$\vartheta = \frac{\vartheta_1 \vartheta_2}{\vartheta_1 + \vartheta_2 - \vartheta_1 \vartheta_2} \quad (27)$$

where  $g$  is the surge coefficient of temperature;  $\vartheta$  is the combined temperature accommodation coefficient; and the accommodation coefficients  $\vartheta_1$  and  $\vartheta_2$  indicate the degree of heat exchange between gas molecules and surfaces.

The average molecular mean free path in the case of molecular flow greatly exceeds the characteristic length, and the corresponding heat transfer of residual gas between parallel plates is described below:

$$Q = \vartheta \cdot \left( \frac{\gamma_{\text{gas}} + 1}{\gamma_{\text{gas}} - 1} \right) \sqrt{\frac{R}{8\pi M_{\text{gas}} T_{\text{ave}}}} \cdot P (T_{s3} - T_{s2}) A_g \quad (28)$$

where  $\gamma_{\text{gas}}$  is the specific heat ratio of residual gas;  $R$  is the universal gas constant,  $R = 8.314 \text{ J} \cdot \text{mol}^{-1} \cdot \text{K}^{-1}$ ;  $M_{\text{gas}}$  is the molecular weight,

$\text{g} \cdot \text{mol}^{-1}$ ; and  $T_{\text{ave}}$  is the average temperature of the two surfaces, K. Based on the above heat transfer in different gas flow states, the thermal resistance of the residual gas ( $R_{\text{gas}}$ ) is expressed in Eq. (29):

$$R_{\text{gas}} = \begin{cases} \frac{L}{K_{\text{gas}}} & l \ll L \\ \frac{4l - 2\vartheta l + \vartheta L}{\vartheta K_{\text{gas}}} & l \approx L \\ \left[ \left( \vartheta \cdot \frac{\gamma_{\text{gas}} + 1}{\gamma_{\text{gas}} - 1} \right) \sqrt{\frac{R}{8\pi M_{\text{gas}} T}} \cdot P \right]^{-1} & l \gg L \end{cases} \quad (29)$$

(4) **Thermal resistance of the sealed edge.** In vacuum glazing, a leak-free hermetic seal is vital for maintaining high vacuum. However, it acts as a heat short circuit, decreasing its overall thermal performance. Simko et al. [89,90] analyzed the heat flow associated with the edge seal in vacuum glazing and proposed a simple analytical model. The formula for the heat flow per unit length of the edge effect is expressed in Eqs. (30) and (31):

$$Q_{\text{edge}} = \frac{k_g t_g (T_{\text{in}} - T_{\text{out}})}{\omega_1 + \omega_2 + \sqrt{k_g t_g / h_i} + \sqrt{k_g t_g / h_o}} \quad (30)$$

$$R_{\text{edge}} = \frac{\omega_1 + \omega_2 + \sqrt{k_g t_g / h_i} + \sqrt{k_g t_g / h_o}}{k_g t_g} \quad (31)$$

where  $Q_{\text{edge}}$  is the heat flow per unit length of the edge effect,  $\text{W} \cdot \text{m}^{-2}$ ;  $R_{\text{edge}}$  is the thermal resistance of the edge,  $\text{m}^2 \cdot \text{K} \cdot \text{W}^{-1}$ ;  $\omega_1$  and  $\omega_2$  represent the distance between the insulation and the edge of the seal on the warm and cold sides, respectively. The above thermal resistances, including outdoor convection thermal resistance ( $R_{\text{co}}$ ), outdoor radiative thermal resistance ( $R_{\text{ro}}$ ), indoor convection thermal resistance ( $R_{\text{ci}}$ ), indoor radiative thermal resistance ( $R_{\text{ri}}$ ) and the thermal resistance of different components in vacuum glazing, are summarized in Table 5.

On the basis of the above analytical method, thermal resistance network models for composite vacuum structures, namely, hybrid, triple, and PV vacuum glazing, were established, as illustrated in Fig. 8 [16,91]. Compared with traditional gas-filled triple glazing, hybrid vacuum glazing offers a lower  $U$ -value and thinner thickness [16], potentially reaching a central  $U$ -value of  $0.26 \text{ W} \cdot \text{m}^{-2} \cdot \text{K}^{-1}$  [48,91]. Tan et al. [45] developed a thermal resistance model for four-layer PV vacuum glazing and evaluated its dynamic thermal performance across different climates in China. Furthermore, Chen et al. [43] evaluated the influences of support pillars' thermal conductivity on the  $U$ -value of laminated PV vacuum glazing via an analytical model. The findings indicated that the central  $U$ -value

**Table 5**  
Heat transfer through different components of the vacuum glazing.

Heat transfer mode	Component	Thermal resistance ( $\text{m}^2 \cdot \text{K} \cdot \text{W}^{-1}$ )
Conduction	Glass panes	$R_g = \frac{t_g}{A_g k_g}$
	Support array	$\lambda^2 \left( 1 + \frac{2k_g h}{k_p \pi a} \right)$
		$R_{\text{pa}} = \frac{2k_g a}{2k_g a}$
	Residual gas	$R_{\text{gas}} = \left[ \left( \vartheta \cdot \frac{\gamma_{\text{gas}} + 1}{\gamma_{\text{gas}} - 1} \right) \sqrt{\frac{R}{8\pi M_{\text{gas}} T}} \cdot P \right]^{-1}$
	Edge seal	$R_{\text{edge}} = \frac{\omega_1 + \omega_2 + \sqrt{k_g t_g / h_i} + \sqrt{k_g t_g / h_o}}{k_g t_g}$
Radiation	Outermost/innermost surface	$R_{\text{ro}} = 1/h_{\text{ro}} R_{\text{ri}} = 1/h_{\text{ri}}$
	Parallel surfaces in vacuum gap	$R_{\text{rad}} = \left( \epsilon_e \cdot \sigma \cdot \frac{T_{s2}^4 - T_{s3}^4}{T_{s2} - T_{s3}} \right)^{-1}$
Convection	Outermost/innermost surface	$R_{\text{co}} = 1/h_{\text{co}} R_{\text{ci}} = 1/h_{\text{ci}}$

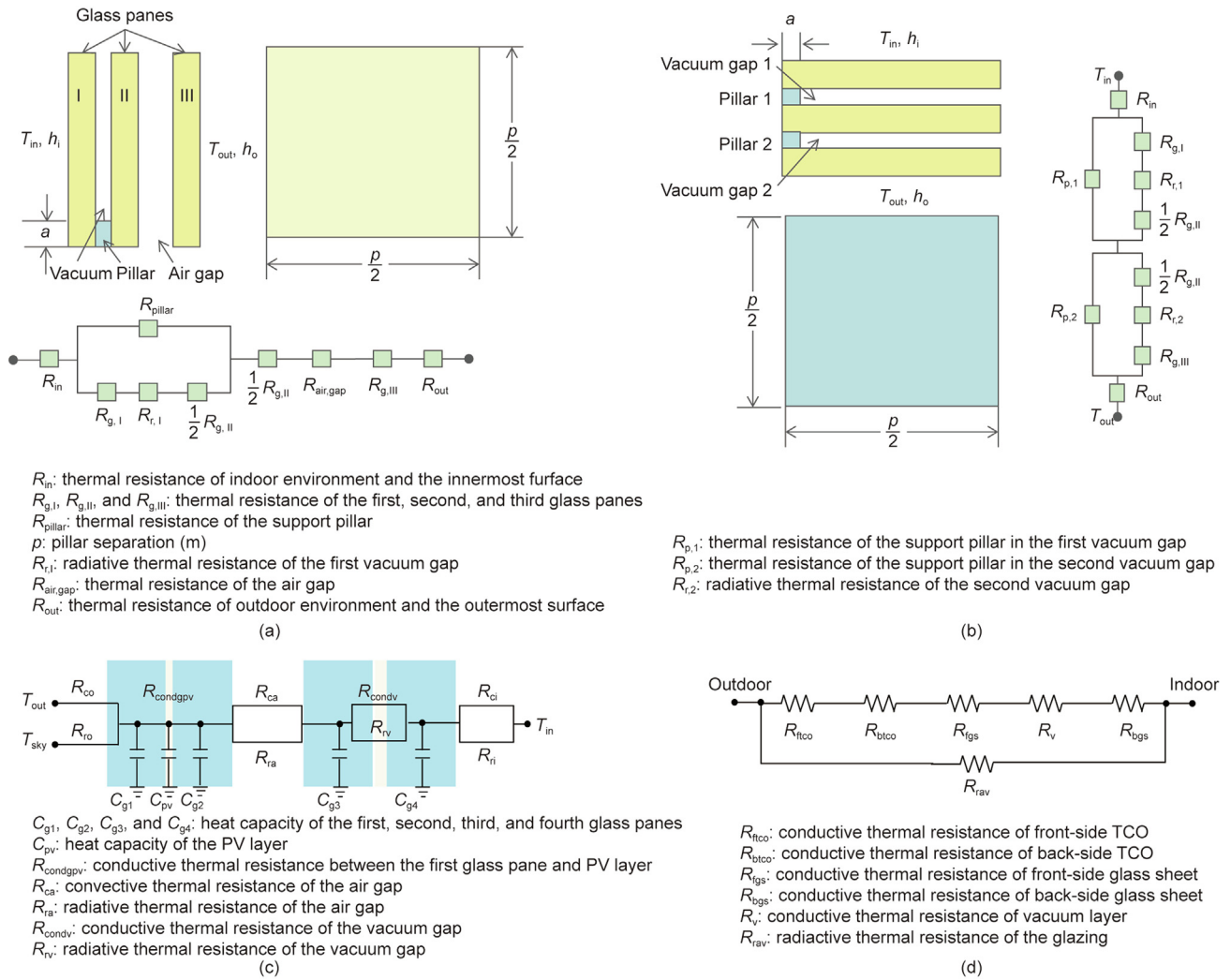


**Fig. 8.** The diagrams of the thermal resistance network of different vacuum glazing structures. (a) Hybrid vacuum glazing; (b) triple vacuum glazing; (c) laminated PV-vacuum glazing; (d) hollow PV-vacuum glazing. TCO: transparent conductive oxide. Reproduced from Refs. [16,91] with permission.

of PV vacuum glazing with aerogel pillars is half that of glazing with steel pillars.

### 3.2. Numerical research

By employing analytical methods, researchers can obtain the  $U$ -value of vacuum glazing and conduct sensitivity analyses. Nonetheless, this method falls short in depicting the surface temperature distribution. Therefore, the finite element method (FEM) and finite volume method (FVM) have been employed to evaluate the performance of various types of vacuum glazing.

#### 3.2.1. Finite element method

The FEM divides a continuous system into subdomains known as finite elements. This computational method is employed to estimate solutions for boundary value problems in partial differential equations. In the case of vacuum glazing, modeling only one quarter of the system is sufficient because of the consideration of symmetry [81,92]. Typically, solid, double-shell-layer, and single-shell-layer models are utilized for stress and thermal analyses of vacuum glazing, as shown in Fig. 9 [93].

Hu et al. [94] carried out a thermal performance analysis on the basis of an FEM of vacuum glazing via MATLAB (developed by the MathWorks Inc., USA), as shown in Fig. 10 [94]. The results revealed that the temperatures of the support pillar and the edge

seal on the warm side were 16.17 and 10.38 °C, respectively, and the corresponding temperatures on the cold side were 4.59 and 7.48 °C, respectively.

Various commercial software packages, such as ABAQUS (Dassault Systemes SE, France), COMSOL Multiphysics (COMSOL Inc., Sweden), ANSYS (ANSYS Inc., USA), and MSC.Marc (MSC Software Inc., USA), were subsequently adopted to perform FEM simulations for the thermal analysis of vacuum glazing. Fang et al. [95] established a finite element model of vacuum glazing using eight-node isoparametric elements. The findings revealed a 16.4% deviation between the experimental and predicted  $U$ -values due to the influence of outgassing. To enhance the analysis and optimize the thermal properties of vacuum glazing, researchers have developed a finite element model in ABAQUS software [86]. An evaluation of the design parameters of vacuum glazing

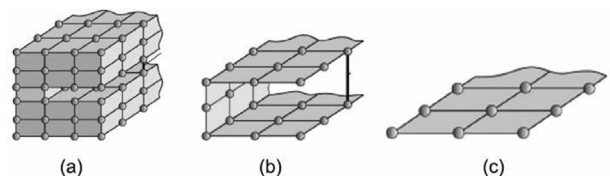


**Fig. 9.** (a) Solid element, (b) double shell-layer element, and (c) single shell-layer element. Reproduced from Ref. [93] with permission.

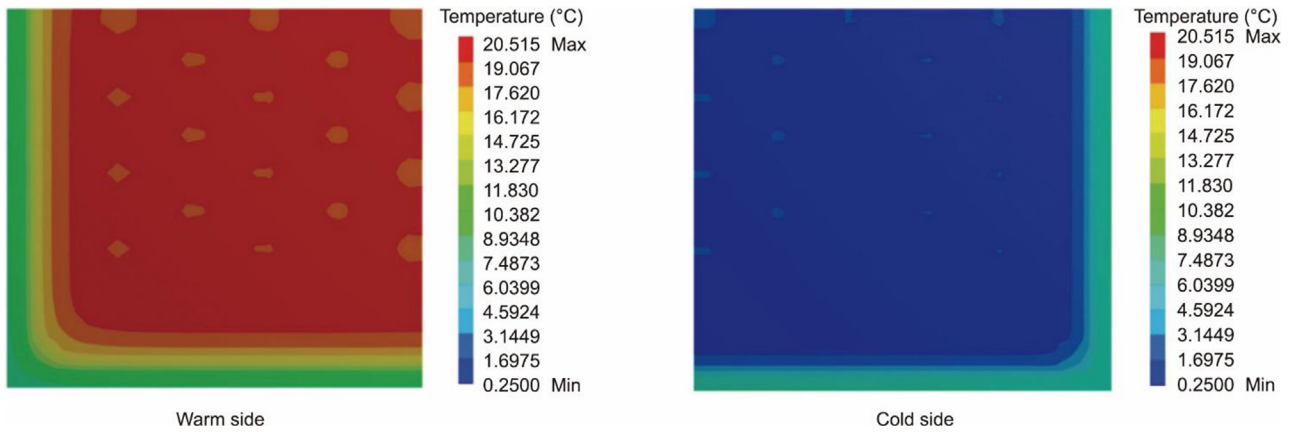


Fig. 10. Finite-element mesh of vacuum glazing (500 mm × 500 mm) and the temperature distribution on both warm and cold surfaces [94].

with respect to its thermal performance revealed that as the vacuum level increased from 0.001 Pa to 100 kPa, the corresponding central  $U$ -value increased to  $2.40 \text{ W}\cdot\text{m}^{-2}\cdot\text{K}^{-1}$  [96]. Chen et al. [43] established an FEM for PV vacuum glazing in COMSOL software and reported that replacing stainless steel support pillars with aerogel materials can decrease the total  $U$ -value by  $0.33 \text{ W}\cdot\text{m}^{-2}\cdot\text{K}^{-1}$ . Furthermore, optimizing the structure of PV vacuum glazing can achieve a  $U$ -value of  $0.23 \text{ W}\cdot\text{m}^{-2}\cdot\text{K}^{-1}$  [97]. Additionally, the thermal characteristics of hybrid and triple vacuum glazing were analyzed via finite element models created in ANSYS and MSC.Marc software, respectively [98,99]. The detailed thermal performance of different vacuum glazing types and their influencing parameters are discussed in Section 5. In addition, the properties of commonly used vacuum glazing materials are summarized in Table 6 [86,100].

### 3.2.2. Finite volume method

The FVM, whose governing equation is the heat diffusion equation, shown in Eq. (32), is an efficient way to analyze thermal performance. This equation is derived by considering Fourier's law and the control volume surface area [91,101]:

$$\frac{\partial^2 T}{\partial x^2} + \frac{\partial^2 T}{\partial y^2} + \frac{\partial^2 T}{\partial z^2} = \frac{1}{\alpha} \frac{\partial T}{\partial \tau} \quad (32)$$

where  $T$  is the temperature;  $\tau$  is the time factor;  $x$ ,  $y$ , and  $z$  are the width, thickness, and height directions of the glazing; and  $\alpha$  is the thermal diffusivity, with  $\alpha = k/(\rho c)$ .  $\rho$  is the density,  $\text{g}\cdot\text{cm}^{-3}$ .

The surface-to-surface radiation model is commonly employed in the FVM modeling process [91,102]. The multizone approach is utilized to construct the 3D model via the design modular tool, which enables independent control over each zone. Cubical pillars are used to represent cylindrical pillars with equivalent cross-sectional areas, ensuring consistent heat transfer amounts. Then, the computational domain is segmented into multiple elements by meshing tools, with a graded mesh employed to increase accuracy [103,104]. The governing equation is solved via the Galerkin approach, and convergence is determined on

the basis of relative residual criteria [105]. Compared with FEM calculations, the FVM model features a narrower equation bandwidth, leading to fewer computational steps and reduced processing time to achieve satisfactory results [103,106]. Consequently, the FVM is widely used for investigating the thermal performance of vacuum glazing.

Using the FVM model for vacuum glazing, Fang et al. [17,44] explored the impacts of glass thickness, emissivity, and other factors on the  $U$ -value. The results in Ref. [102] indicated that when the glass pane thickness increased from 3 to 6 mm, the  $U$ -value of vacuum glazing with dimensions of 300 mm (length) × 300 mm (width) increased by  $0.13 \text{ W}\cdot\text{m}^{-2}\cdot\text{K}^{-1}$  because of lateral heat conduction. The  $U$ -value of vacuum glazing with a size of 1 m (length) × 1 m (width) decreased since the glass thickness increased from 2 to 3.5 mm. This is because the increase in thermal resistance across glass panes is greater than the rate of lateral heat conduction when the thickness of the glass pane is increased within this size range. Furthermore, increasing the thickness does not result in any extra reduction in the  $U$ -value, as shown in Fig. 11 [44].

Fang et al. [103] compared the temperature distributions between vacuum glazing with tempered glass and that with annealed glass, and the results showed that the tempered glass exhibits better thermal performance than annealed glass. For triple vacuum glazing, Fang et al. [91] noted that despite significant variations in the conductivity of different sealing materials, the  $U$ -value difference was  $0.1 \text{ W}\cdot\text{m}^{-2}\cdot\text{K}^{-1}$ . Furthermore, the accuracy of the FVM model was verified through a hot box experiment, which demonstrated commendable agreement, with a mere 3% relative error [101].

## 4. Experimental research

### 4.1. Hot box apparatus

To assess the  $U$ -value of vacuum glazing and validate corresponding analytical and numerical models, Fang et al. [95]

Table 6  
Material properties of vacuum glazing components used in finite element models [86,100].

Material	Density ( $\text{g}\cdot\text{cm}^{-3}$ )	Elastic modulus (GPa)	Poisson's ratio	Specific heat ( $\text{J}\cdot\text{kg}^{-1}\cdot\text{K}^{-1}$ )	Expansion coefficient ( $10^{-6} \text{ K}^{-1}$ )	Conductivity ( $\text{W}\cdot\text{m}^{-1}\cdot\text{K}^{-1}$ )
Glass	2.500	73.000	0.2200	800	7.00	1.000
Ceramic	3.000	350.000	0.2000	900	6.60	1.100
Aerogel	0.003	0.143	0.0003	1	0.12	0.024
Indium alloy	6.440	144.000	0.4500	400	1.50	83.700
Stainless-steel	7.930	200.000	0.2500	460	17.00	20.000
Aluminium alloy	2.810	70.000	0.3300	900	12.00	201.000

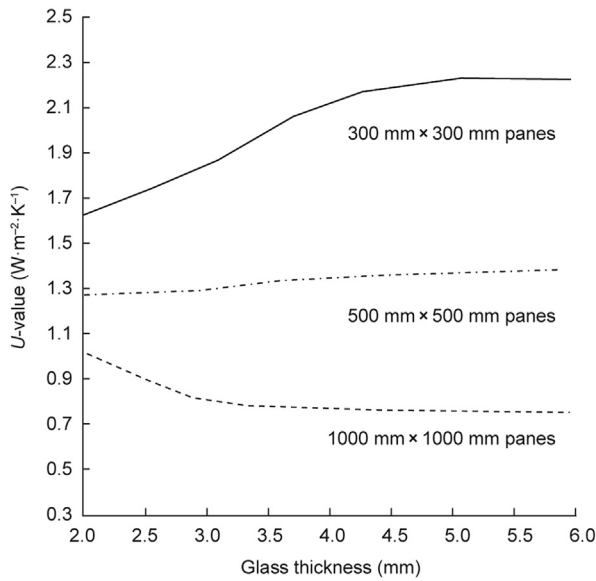


Fig. 11. The impacts of the glass thickness on  $U$ -value of vacuum glazing. Reproduced from Ref. [44] with permission.

designed and built a guarded hot box apparatus, as shown in Fig. 12 [95]. The guarded hot box device comprises a metering box, an environmental box, and a guarded chamber [107]. The metering box is equipped with an electric heating device that regulates the temperature to simulate indoor conditions, which are generally maintained at 20 °C. The environmental box emulates winter outdoor conditions, and its temperature is usually maintained at -20 °C through a cooling fan. The temperature of the guarded box is aligned with that of the metering box to minimize heat transfer ( $Q_b$ ). The sample is installed on the mask wall, and the heat flow via the mask wall ( $Q_m$ ) is obtained by measuring the mean surface temperatures. The heat flow through the edge ( $Q_e$ ) is assessed via standard glazing samples with known thermal conductivity. Thus, the heat transfer through vacuum glazing can be calculated [108]:

$$Q_s = Q_{input} - Q_b - Q_m - Q_e \tag{33}$$

$$U = \frac{Q_s}{A_g(T_1 - T_2)} \tag{34}$$

where  $Q_{input}$  is the input power of the electric heating instrument,  $W$ ;  $Q_s$  is the heat flow through the sample,  $W$ ;  $A_g$  is the area of the glazing sample,  $m^2$ ; and  $T_1$  and  $T_2$  are the air temperatures of the metering boxes and environmental boxes, respectively, °C.

By employing guarded hot box apparatuses, researchers have conducted heat transfer performance measurements on various vacuum glazing types, validating their respective models [109]. Fang et al. [101] measured the  $U$ -value of hybrid vacuum glazing and validated its FVM numerical model. The central and total  $U$ -values of the hybrid vacuum glazing were 0.66 and 0.91  $W \cdot m^{-2} \cdot K^{-1}$ , respectively. This shows a strong alignment between the numerical and experimental data, with relative errors of 3% for the central  $U$ -value and 1% for the total  $U$ -value. Additionally, Park et al. [110] investigated different hybrid vacuum glazing configurations with various low-E coating locations, resulting in  $U$ -values ranging from 1.369 to 0.428  $W \cdot m^{-2} \cdot K^{-1}$ . In addition, researchers have analyzed the heat transfer coefficients of triple, EC and PV vacuum glazing via a hot box device. For triple vacuum glazing, its central and total  $U$ -values increased by 0.24 and 0.26  $W \cdot m^{-2} \cdot K^{-1}$ , respectively, with distinct low-E coating arrangements [111]. Papaefthimiou et al. [53] reported that the central  $U$ -value of EC vacuum glazing with dimensions of 400 mm (length)  $\times$  400 mm (width) is 1.18  $W \cdot m^{-2} \cdot K^{-1}$ . Tan et al. [112] established an analytical model of PV vacuum glazing and validated it through a guarded hot box device, which demonstrated close agreement (relative error = 3%) between experimental and simulated  $U$ -values. The  $U$ -values of different windows measured by the hot box apparatus were summarized in Table 7 [53, 101, 110–112].

Researchers have not only tested the heat transfer coefficient of vacuum glazing and verified models but have also examined the influence of coating emissivity, rebate width, and other factors on the  $U$ -value via a hot box device. Fang et al. [17] evaluated the impact of low-E coatings on the  $U$ -value. The results revealed that when the emissivity decreased from 0.16 to 0.04, the central and total  $U$ -values decreased by 0.20 and 0.15  $W \cdot m^{-2} \cdot K^{-1}$ , respectively. Notably, coating emissivity had a more obvious influence on the central  $U$ -value than on the total  $U$ -value because of the edge effect. Furthermore, Fang et al. [113] analyzed the effects of frame width and rebate depth on the  $U$ -value on the basis of experimental data. The findings indicated that as the frame width increased

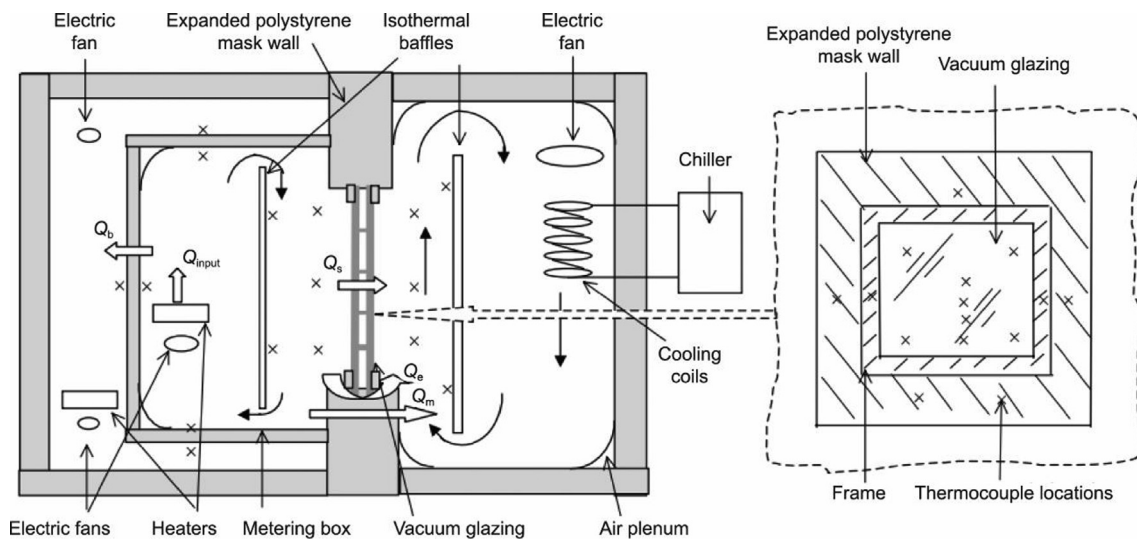


Fig. 12. Schematic diagram of the guarded hot box device. Reproduced from Ref. [95] with permission.

**Table 7**  
The  $U$ -values of different vacuum glazing using hot box apparatus.

Ref.	Type	$U$ -value ( $\text{W}\cdot\text{m}^{-2}\cdot\text{K}^{-1}$ )	
		Central	Total
Fang et al. [101]	Hybrid vacuum	0.66	0.91
Park et al. [110]	Hybrid vacuum	0.43–1.37	–
Fang et al. [111]	Triple vacuum	0.53–0.77	0.88–1.14
Papaefthimiou et al. [53]	EC-vacuum	1.18	–
Tan et al. [112]	PV-vacuum	–	0.92

from 40 to 60 mm, the  $U$ -value decreased by 10.2%. Meanwhile, the vacuum glazing was installed in a frame with depths ranging from 16 to 25 mm, resulting in an 8.9% reduction in the  $U$ -value. This study revealed that while the sealing edge may have a negative effect on the thermal performance of vacuum glazing, this effect could be mitigated by increasing the window frame width and rebated depth. Additionally, the fabrication process affects the thermal performance of vacuum glazing. Zhao et al. [34] found that the vacuum glazing created through the two-stage fabrication process has a lower  $U$ -value than that produced via the single-stage fabrication process.

#### 4.2. Indoor and outdoor test rigs

Although hot box experiments are precise and efficient, their high cost and lengthy testing duration restrict their widespread utilization. Consequently, researchers have developed simplified indoor [114,115] or outdoor test rigs to carry out heat transfer performance experiments, as depicted in Fig. 13 [49]. Typically, the test cell was made of 10 cm-thick polystyrene with a glazing sample embedded in the top or sides [76]. The thermocouples are strategically positioned on the glass surfaces and within the test chamber to monitor the temperatures accurately. The heat transfer of the glazed sample is obtained via a heat flow meter for thermal performance assessment. Further details regarding the instruments and equipment utilized in these test setups can be found in Table 8.

Qiu et al. [116] measured the heat flux through PV vacuum glazing with a test cell, which yielded a  $U$ -value of  $1.5 \text{ W}\cdot\text{m}^{-2}\cdot\text{K}^{-1}$  [117]. Ghosh et al. [49] demonstrated that the  $U$ -values of SPD vac-

uum glazing in the transparent and tinted states were  $1.16$  and  $1.01 \text{ W}\cdot\text{m}^{-2}\cdot\text{K}^{-1}$ , respectively. The  $U$ -values of PDLC vacuum glazing in the on and off states were  $1.09$  and  $1.01 \text{ W}\cdot\text{m}^{-2}\cdot\text{K}^{-1}$ , respectively [51]. The above results indicate that the  $U$ -value of the vacuum glazing samples tested in these rigs is relatively high. This is because the test cell is usually small, with dimensions of approximately  $300 \text{ mm}$  (length)  $\times$   $300 \text{ mm}$  (width)  $\times$   $300 \text{ mm}$  (height), which results in an obvious edge effect.

### 5. Thermal performance and sensitivity analysis of vacuum glazing

#### 5.1. Comparative analysis of different structures

On the basis of the theoretical analysis, numerical simulation, and experimental methods outlined in Section 3.1, researchers have thoroughly examined the thermal performance of different configurations of vacuum glazing. Table 9 lists typical structures of vacuum glazing units alongside their corresponding heat transfer coefficients. The  $U$ -value of conventional vacuum glazing ranges from  $1.05$  to  $1.40 \text{ W}\cdot\text{m}^{-2}\cdot\text{K}^{-1}$ . For hybrid vacuum glazing, Fang et al. [118] evaluated the influence of insulation gap placement on the  $U$ -value, revealing values of  $0.33$  and  $0.49 \text{ W}\cdot\text{m}^{-2}\cdot\text{K}^{-1}$  when moving from the outside to the inside. Shi et al. [98] reported that vacuum glazing with two low-E coatings with  $0.07$  emissivity on vacuum gap surfaces results in a  $U$ -value of  $0.61 \text{ W}\cdot\text{m}^{-2}\cdot\text{K}^{-1}$ . Reducing the emissivity to  $0.016$  can further reduce the  $U$ -value to  $0.26 \text{ W}\cdot\text{m}^{-2}\cdot\text{K}^{-1}$ , as depicted in Fig. 14 [119]. Additionally, the type and thickness of the insulating layer medium also affect the thermal performance of the hybrid vacuum glazing, as explained in Section 5.2.

Among the vacuum glazing designs discussed, triple vacuum glazing offers the best thermal insulation. Manz et al. [48] designed triple vacuum glazing to achieve a center-of-glazing  $U$ -value below  $0.10 \text{ W}\cdot\text{m}^{-2}\cdot\text{K}^{-1}$  by utilizing advanced ceramic support pillars and four low-E coatings with an emissivity of  $0.03$ . According to Fang et al. [91], the central  $U$ -value of a  $1000 \text{ mm}$  (length)  $\times$   $1000 \text{ mm}$  (width) triple vacuum glazing system, which includes three glass panes, four low-E coatings, and stainless-steel support pillars, is  $0.26 \text{ W}\cdot\text{m}^{-2}\cdot\text{K}^{-1}$ . In addition, Fang et al. [111] asserted that placing a low-E coating in each of the two vacuum gaps is more effective at reducing the  $U$ -value than having two coatings within one vacuum gap.

For tinted vacuum and PV vacuum glazing, the advantages include not only achieving a significantly lower heat transfer coefficient but also actively modulating the SHGC or harnessing incident solar radiation while maintaining the desired  $U$ -value. The visible transmittance of the SPD vacuum glazing varies from 2% (switch off/opaque) to 38% (switch on/transparent) [120]. EC vacuum glazing measuring  $400 \text{ mm}$  (length)  $\times$   $400 \text{ mm}$  (width) exhibits a total  $U$ -value of approximately  $1.0 \text{ W}\cdot\text{m}^{-2}\cdot\text{K}^{-1}$ , with a dynamic transmission ranging from 38% in its transparent state to 2% in its fully tinted state [49]. The EC layer was suggested to face the outdoor environment to avoid overheating [121]. The reference PV vacuum glazing sample with aerogel support pillars has a higher  $U$ -value of  $0.68 \text{ W}\cdot\text{m}^{-2}\cdot\text{K}^{-1}$  than the sample with stainless-steel support pillars [122]. This is because the latter uses a coating with lower emissivity. Ghosh et al. [123] used an analytical model to determine the overall  $U$ -value of PV vacuum glazing, which was  $0.8 \text{ W}\cdot\text{m}^{-2}\cdot\text{K}^{-1}$ . Radwan et al. [124] reported that the central  $U$ -value of PV vacuum glazing with dimensions of  $150 \text{ mm}$  (length)  $\times$   $150 \text{ mm}$  (width) was  $1.2 \text{ W}\cdot\text{m}^{-2}\cdot\text{K}^{-1}$ . Various components exert differing degrees of influence on the  $U$ -value of vacuum glazing. Consequently, a parameter sensitivity analysis of the  $U$ -value of vacuum glazing is carried out in Section 5.2.

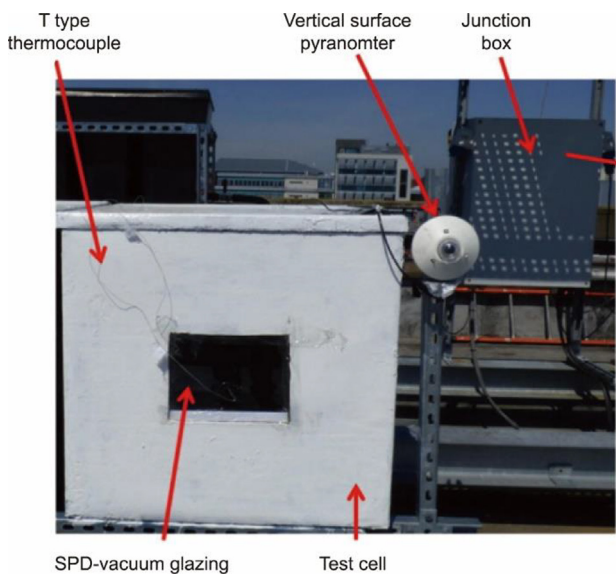


**Fig. 13.** Schematic diagram of the test rig. Reproduced from Ref. [49] with permission.

**Table 8**  
Summary of key experimental instruments used in the test cell [49,51,116].

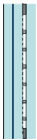
Equipment	Function	Manufacture	Country	Type	Accuracy/sensitivity
Polystyrene Thermocouples	Preparation of test cell Measuring temperature	—	—	—	—
		RS Components Ltd.	UK	T-type	±0.2 °C
		OMEGA Engineering Inc.	USA	T-type	±0.5 °C
Heat flux meter Pyranometers	Measuring heat flow Measuring solar radiation	Captec Enterprise	France	K-type	±1.5 °C
		EKO Instruments Co., Ltd.	Japan	RS-30	About 5 μV·W <sup>-1</sup> ·m <sup>2</sup>
		Kipp & Zonen, Inc.	The Netherlands	MS-802	About 7 μV·W <sup>-1</sup> ·m <sup>2</sup>
		Kipp & Zonen, Inc.	The Netherlands	SMP 11	Non-linearity < 0.2%
Data logger	Collecting and recording	Graphtec Corporation	Japan	CMP 6	About 8 μV·W <sup>-1</sup> ·m <sup>2</sup>
		Delta-T Devices Ltd.	UK	GL840	1 μA and 0.1 °C
		Keysight Technologies	USA	Delta T type	—
		Pico Technology Ltd.	UK	Keysight Agilent 34970A	±1.5 and ±190 μV
		—	—	Pico data logger	—

**Table 9**  
Summary of thermal performance of popular composite vacuum glazing.

Type	Ref.	Dimension (length (mm) × width (mm))	Glass thickness (mm)	Coating/film	Cavity	Support pillar		Sealant	U-value (W·m <sup>-2</sup> ·K <sup>-1</sup> )		
						Material	Layout		Material	Width (mm)	Center
<b>Double-pane</b> 	Fang et al. [95]	500 × 500	4 + 4	—	One vacuum gap	Stainless-steel	H = N.A. D = 0.40 mm S = 25 mm	Indium	6 10	— —	1.21 1.28
	Wang et al. [100]	400 × 400	4 + 4	Two low-E coatings Emissivity = 0.15	One vacuum gap	Inconel 718	H = 0.20 mm D = 0.30 mm S = 25 mm	Indium	6	—	1.40
	Memon et al. [104]	300 × 300	4 + 4	Three low-E coatings Emissivity = 0.15	One vacuum gap	Stainless-steel	H = 0.15 mm D = 0.30 mm S = 24 mm	CS186	10	0.91	1.05
<b>Triple</b> 	Memon [37]	300 × 300	4 + 4 + 4	Three low-E coatings Emissivity = 0.15	Two vacuum gaps	Stainless-steel	H = 0.25 mm D = 0.30 mm S = 24 mm	CerasolzerCS-186	10	0.33	1.05
	Manz et al. [48]	—	6 + 4 + 6	Four low-E coatings Emissivity = 0.03	Two vacuum gaps	Stainless-steel	H = 0.20 mm D = 0.30 mm S = 35 mm	—	—	0.20	—
	Fang et al. [91]	1000 × 1000	4 + 4 + 4	Four low-E coatings Emissivity = 0.03	Two vacuum gaps	Stainless-steel	H = 0.12 mm D = 0.30 mm S = 25 mm	Indium	6	0.26	0.49
<b>Hybrid</b> 	Shi et al. [98]	1000 × 1000	5 + 5 + 5	Two low-E coatings Emissivity = 0.07	One argon gap One vacuum gap	1Cr18Ni9	H = 0.20 mm D = 0.60 mm S = 30 mm	—	5	—	0.61
	Fang et al. [118]	400 × 400	4 + 4 + 4	—	One air gap One vacuum gap	—	—	Indium	—	0.33	—
	Baek and Kim [119]	—	4 + 3 + 3	Two low-E coatings Emissivity = 0.016	One CO <sub>2</sub> gap One vacuum gap	—	H = 0.20 mm D = 0.40 mm S = 30 mm	Indium	15	0.26	—

(continued on next page)

Table 9 (continued)

Type	Ref.	Dimension (length (mm) × width (mm))	Glass thickness (mm)	Coating/film	Cavity	Support pillar		Sealant		U-value ( $W \cdot m^{-2} \cdot K^{-1}$ )	
						Material	Layout	Material	Width (mm)	Center	Total
<b>Tinted</b> 	Papeafthimiou et al. [53]	400 × 400	—	One low-E coating Emissivity = 0.06	One vacuum gap One EC laminate	—	H = 0.15 mm D = 0.40 mm S = 25 mm	—	—	0.86	—
	Fang and Eames [125]	400 × 400	—	Two low-E coatings Emissivity = 0.02	One vacuum gap One EC laminate	—	H = 0.12 mm D = 0.32 mm S = 25 mm	Metal	6	0.51	1.06
	Ghosh et al. [49,126]	280 × 210	—	—	One vacuum gap One SPD laminate	—	—	—	—	—	—
<b>PV</b> 	Tan et al. [112]	1100 × 600	5 + 5 + 3 + 3	One low-E coating Emissivity = 0.21	One Air gap One vacuum gap	Stainless-steel	H = 0.28 mm D = 0.35 mm S = 40 mm	Indium	—	—	0.92
	Jarimi et al. [122]	300 × 300	4 + 4	One low-E coating Emissivity = 0.4	One vacuum gap	Aerogel	H = 0.30 mm D = 1.00 mm S = 47 mm	—	8	—	1.60
	Qiu and Yang [78,127]	300 × 300	3 + 3 + 3 + 3	One low-E coating Emissivity = 0.042	One vacuum gap One PV laminate	Stainless-steel	H = 0.10 mm D = 0.10 mm S = 50 mm	—	—	0.557	—

H = height, D = diameter, and S = spacing.

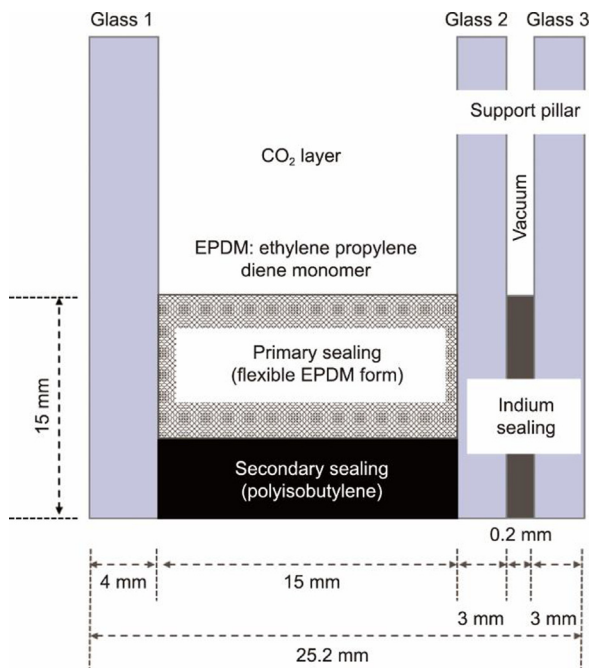


Fig. 14. Optimal design of hybrid vacuum glazing [119].

### 5.2. Sensitivity analysis for U-values

From the above analysis, even with the same category of vacuum glazing, the heat transfer coefficient can vary considerably due to differences in structure, material, and other factors. Therefore, this study provides a comprehensive summary of the factors influencing the thermal performance of vacuum glazing and their respective influence mechanisms, as presented in Table 10. With respect to the manufacturing technique, Zhao et al. [34] reported that the U-value of vacuum glazing produced via the two-step method is 0.2  $W \cdot m^{-2} \cdot K^{-1}$  lower than that of the one-step method. Additionally, the dimensions of vacuum glazing have a considerable effect on its thermal performance. Katsura et al. [102] explored the influence of vacuum glazing dimensions on thermal performance. They discovered that vacuum glazing with dimensions of 300, 500, and 1000 mm had U-values of 1.87, 1.25, and 0.85  $W \cdot m^{-2} \cdot K^{-1}$ , respectively. Similarly, Jarimi et al. [122] reported that the U-values of PV vacuum glazing with specified dimensions were 0.64, 0.58, and 0.55  $W \cdot m^{-2} \cdot K^{-1}$ . Comparative analysis suggests that larger vacuum glazing sizes result in better performance because of the more pronounced edge effect in smaller vacuum glazing [104].

With respect to glass panes, Fang and Arya [103] analyzed the impact of tempered and annealed glass on the thermal performance of vacuum glazing. The findings demonstrated a 47.4%

**Table 10**  
Summary of the factors affecting vacuum glazing’s thermal performance.

Components	Factors	References	Method	Results	Conclusions
–	Fabrication method	Zhao et al. [34]	Hot box	The $U$ -value of the vacuum glazing produced via the two-stage method is $0.2 \text{ W}\cdot\text{m}^{-2}\cdot\text{K}^{-1}$ lower than that prepared by the one-stage method	–
–	Dimension	Katsura et al. [102]	FVM	The $U$ -value of vacuum glazing decreased by $1.02 \text{ W}\cdot\text{m}^{-2}\cdot\text{K}^{-1}$ as the dimension increases from 300 to 1000 mm	The dimension of vacuum glazing has a significant influence on its thermal performance, and the larger size leads to a lower $U$ -value
Glass	Thickness	Memon et al. [104]	FVM	The central $U$ -value decreases by 5.5% when the size rises from 300 to 400 mm	The $U$ -value of vacuum glazing rises slowly and linearly with glass thickness, with larger sizes showing a slower rate of increase
		Jarimi et al. [122]	Hot box	PV-vacuum glazing with sizes of 300 and 1000 mm yield $U$ -values of $0.64$ and $0.55 \text{ W}\cdot\text{m}^{-2}\cdot\text{K}^{-1}$	
	Zhu et al. [128]	FEM	Compared with 300 and 500 mm dimension, the $U$ -value of 1000 mm vacuum glazing can be decreased by $2/3$ and $1/2$		
	Fang et al. [44]	FVM	The heat transfer coefficient of vacuum glazing increases by 24% as the glass thickness rises from 3 to 6 mm		
Thermal conductivity	Type	Zhu et al. [128]	FEM	When the thickness increases from 2 to 6 mm, the $U$ -value of the vacuum glazing has a reduction of $0.2 \text{ W}\cdot\text{m}^{-2}\cdot\text{K}^{-1}$	The $U$ -value of PV-vacuum glazing linearly rises with the glass pane’s thermal conductivity
		Huang et al. [97]	FEM	When glass thermal conductivity rises from 0.3 to $1.2 \text{ W}\cdot\text{m}^{-2}\cdot\text{K}^{-1}$ , the corresponding $U$ -value of PV-vacuum glazing increased by $0.4 \text{ W}\cdot\text{m}^{-2}\cdot\text{K}^{-1}$	
Insulating cavity	Thickness	Fang and Arya [103]	FVM	Compared to the double-pane vacuum glazing made of annealed glass, the utilization of tempered glass can reduce the $U$ -value by 47.4%	Tempered glass is more conducive to reducing the $U$ -value due to its higher strength
		Huang et al. [97]	FEM	The $U$ -value of the PV vacuum glazing has a reduction of $0.2 \text{ W}\cdot\text{m}^{-2}\cdot\text{K}^{-1}$ when the width of air gap increases from 3 to 15 mm	When the insulating gap thickness reached 15mm, the $U$ -value began to decrease, though very slowly
	Medium	Location	Baek and Kim [119]	WINDOW	When the width of the $\text{CO}_2$ cavity is 15 mm, the $U$ -value of the hybrid vacuum glazing can be reduced to $0.259 \text{ W}\cdot\text{m}^{-2}\cdot\text{K}^{-1}$
Baek and Kim [119]			WINDOW	The $U$ -value of hybrid vacuum glazing injected with Krypton gas is lower than that with air and argon gas	
Vacuum cavity	Vacuum degree	Fang et al. [29,118]	FEM	When the insulating cavity of hybrid vacuum glazing faces outdoors and the vacuum cavity faces indoors, the $U$ -value reduced by 10%	Setting the insulating gap as the outer cavity can better improve the thermal insulation performance
		Memon et al. [96]	FEM	The central and total $U$ -values of the triple vacuum glazing increase by 2.12 and $1.64 \text{ W}\cdot\text{m}^{-2}\cdot\text{K}^{-1}$ when the pressure rises from 0.001 Pa to 100 kPa	The vacuum pressure must be below 0.1 Pa for quelling gaseous heat conduction for a long time
		Katsura et al. [102]	FVM	Comparing the vacuum glazing to double-pane glazing, the $U$ -value is reduced by 51.4%, 48.3%, and 29.4% at vacuum pressures of 0.1, 1.0, and 10.0 Pa	
Support pillar	Material	Chen et al. [43]	FEM	Using an aerogel support pillar instead of a stainless-steel support pillar leads to a $0.33 \text{ W}\cdot\text{m}^{-2}\cdot\text{K}^{-1}$ reduction of PV vacuum glazing’s $U$ -value	The $U$ -value can be effectively reduced by 20% by substituting an aerogel support pillar for the conventional stainless steel support pillar
		Jarimi et al. [122]	FEM	The $U$ -value increased by 40% as the support pillar thermal conductivity rises from 1 to $50 \text{ W}\cdot\text{m}^{-1}\cdot\text{K}^{-1}$	
	Cuce and Riffat [129]	FVM	The $U$ -value of vacuum glazing decreased by 44% with the replacement of aerogel support pillars		
Low-E coating	Geometry	Zhu et al. [86]	FEM	The arrangement of horizontal cylindrical pillars has been demonstrated to improve thermal performance, leading to a $U$ -value reduction of over 25% compared to vertical cylinders	–
		Shi et al. [98]	Hot box	Adding a second low-E coating reduces the $U$ -value of hybrid vacuum glazing by $0.12 \text{ W}\cdot\text{m}^{-2}\cdot\text{K}^{-1}$	Using two low-E coatings improves glazing thermal performance, but only slightly when the emissivity is near to 0.02
		Fang and Eames [125]	FVM	When the emissivity reduces from 0.2 to 0.02, the $U$ -value drops by 52.5% and 35.7% with one and two low-E coatings applied	
Sealant	Temperature	Park et al. [110]	Hot box	The $U$ -value of vacuum glazing with two low-E coatings near the cold side was $0.25 \text{ W}\cdot\text{m}^{-2}\cdot\text{K}^{-1}$ , but increased to $0.33 \text{ W}\cdot\text{m}^{-2}\cdot\text{K}^{-1}$ when placed near the warm side	The low-E coating on the vacuum gap outperforms that on the insulating gap
		Fang et al. [111]	FVM		
	Material	Width	Miao et al. [36]	Hot box	The vacuum glazing, fabricated at a sealing temperature of $500 \text{ }^\circ\text{C}$ , has a $U$ -value of $0.92 \text{ W}\cdot\text{m}^{-2}\cdot\text{K}^{-1}$
Fang et al. [91]			FEM	The vacuum glazing with indium sealant has a higher $U$ -value of $0.01 \text{ W}\cdot\text{m}^{-2}\cdot\text{K}^{-1}$ compared to SG sealant	–
		Zhu et al. [128]	FEM	Reducing the sealing edge width from 12mm to 4mm results in a 20.3% decrease of vacuum glazing’s $U$ -value	The $U$ -value of vacuum glazing decreases linearly as the sealing edge width narrows

reduction in the  $U$ -value when tempered glass was used because its mechanical strength is 4–10 times greater than that of annealed glass. This results in fewer support pillars and diminished thermal conduction. In addition, researchers have investigated the influ-

ence of the glass thickness and thermal conductivity on the  $U$ -value, as shown in Fig. 15 [44,97]. As the glass thickness increases from 2 to 6 mm, the  $U$ -value of vacuum glazing with dimensions of 300, 500, and 1000 mm increases by 0.332, 0.220, and

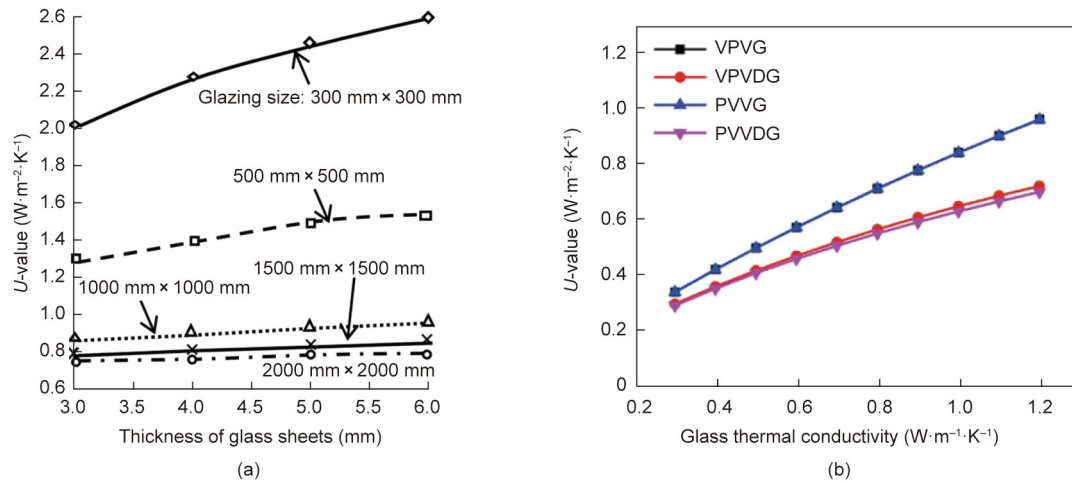


**Fig. 15.** (a) The impact of thickness of the glass panes on the thermal performance. (b) The impact of conductivity of the glass panes on the thermal performance of PV vacuum glazing with the vacuum layer facing outdoors (VPVG), PV vacuum double glazing with the vacuum layer facing outdoors (VPVDG), PV vacuum glazing with the PV layer facing outdoors (PVVG), and PV vacuum double glazing with the PV layer facing outdoors (PVVDG). Reproduced from Refs. [44,97] with permission.

0.132 W·m<sup>-2</sup>·K<sup>-1</sup>, respectively [128]. Additionally, the results indicated minimal variation in the *U*-value resulting from the glass thickness when the glazing size was 2000 mm (length) × 2000 mm (width) [45]. Consequently, the *U*-value of vacuum glazing appears to increase linearly with the thermal conductivity of the glass pane. Additionally, thinner glass panes result in a lower *U*-value [97].

For hybrid vacuum glazing, Fang et al. [118] investigated the impact of insulating cavity placement on the *U*-value, revealing superior thermal performance when the vacuum layer faces a warmer environment. In winter, the hybrid vacuum glazing had *U*-values of 0.49 and 0.33 W·m<sup>-2</sup>·K<sup>-1</sup> when the insulating cavity was positioned closer to the cold and warm environments. Additionally, researchers have investigated the influence of insulation gap thickness on the *U*-value of hybrid and PV vacuum glazing, as shown in Fig. 16 [97,119]. Huang et al. [97] reported that increasing the air cavity width from 3 to 15 mm led to a 0.2 W·m<sup>-2</sup>·K<sup>-1</sup> reduction in the *U*-value of the PV vacuum glazing. Similarly, Baek and Kim [119] noted that when the insulating gap thickness reached 15 mm, the *U*-value of hybrid vacuum glazing started to decrease more gradually.

Another important factor affecting the *U*-value of vacuum glazing is the pressure within the vacuum cavity. Memon et al. [96] explored the impact of vacuum pressure on the thermal perfor-

mance of triple vacuum glazing. As the pressure increased from 0.001 Pa to 100 kPa, the central and total *U*-values rose from 0.28 and 0.94 W·m<sup>-2</sup>·K<sup>-1</sup> to 2.40 and 2.58 W·m<sup>-2</sup>·K<sup>-1</sup>, respectively. Compared with conventional double glazing, vacuum glazing at pressures of 0.1, 1.0, and 10.0 Pa can reduce the *U*-value by approximately 51.4%, 48.3%, and 29.4%, respectively [102].

With advancements in material technology, researchers have turned to higher-performance support pillars to enhance the thermal performance of vacuum glazing [130]. Zhu et al. [86] evaluated the influence of support pillar material on the thermal performance of vacuum glazing. The results indicated that increasing the conductivity of support pillars from 1 to 50 W·m<sup>-1</sup>·K<sup>-1</sup> resulted in a 40% increase in the *U*-value, which was 24 times greater than the increase from 50 to 999 W·m<sup>-1</sup>·K<sup>-1</sup>. Specifically, by substituting aerogels for stainless steel pillars, the *U*-values of vacuum glazing and PV vacuum glazing decreased by 44.2% and 17.3%, respectively [43,129].

With respect to the impact of a low-E coating on the thermal performance of vacuum glazing, Shi et al. [98] used a hot box device to analyze the *U*-values of hybrid vacuum glazing with different low-E coating positions, as shown in Table 11. Compared with the argon gap, placing the low-E coating in the vacuum cavity results in a 0.84 W·m<sup>-2</sup>·K<sup>-1</sup> reduction in the *U*-value of vacuum glazing. Additionally, the *U*-value can be decreased to

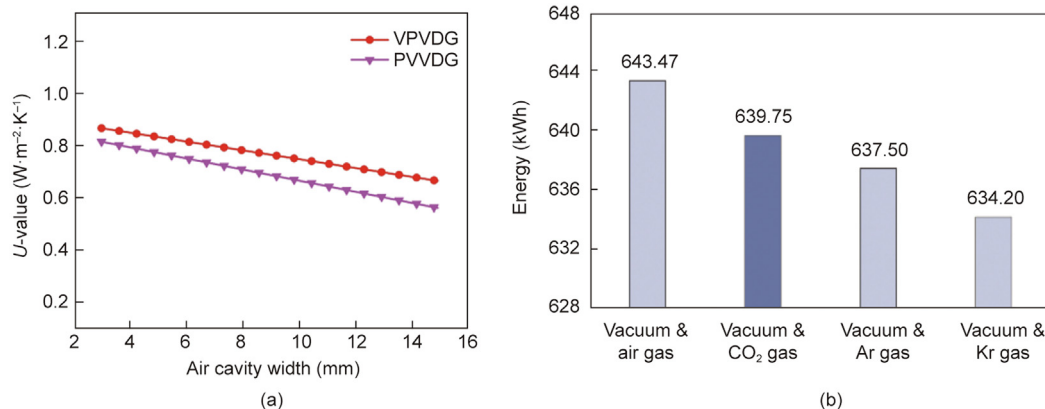


**Fig. 16.** (a) The impacts of insulating cavity thickness on the thermal performance. (b) The impact of insulating cavity types on the thermal performance. Reproduced from Refs. [97,119] with permission.

**Table 11**  
Experimental  $U$ -values of hybrid vacuum glazing.

Case	Experimental $U$ -value ( $W \cdot m^{-2} \cdot K^{-1}$ )
Without low-E coating	1.83
Low-E coating arranged on the surface near the insulating cavity	1.57
Low-E coating arranged on the surface near the vacuum cavity	0.73
Low-E coatings arranged on both sides of the vacuum cavity	0.61

0.61  $W \cdot m^{-2} \cdot K^{-1}$  by applying two low-E coatings to the vacuum gap.

For triple vacuum glazing, as listed in Table 12, Fang et al. [111] reported that the use of two low-E coatings in two vacuum cavities surpasses the use of two coatings in a single vacuum cavity. Low-E coatings with 0.03 emissivity in each cavity lead to a  $U$ -value of 0.25  $W \cdot m^{-2} \cdot K^{-1}$ . However, when both coatings were placed in the vacuum cavity adjacent to the warmer side, the corresponding  $U$ -value was 0.33  $W \cdot m^{-2} \cdot K^{-1}$ . Fang and Eames [125] analyzed the impacts of the emissivity of a low-E coating on the  $U$ -value of vacuum glazing via the FEM. The results indicated that as the emissivity of the low-E coating decreased from 0.2 to 0.02, the central  $U$ -value of vacuum glazing decreased by around 40%. When two low-E coatings were used, the reduction in the  $U$ -value was 0.30  $W \cdot m^{-2} \cdot K^{-1}$ . Therefore, with a low-E coating emissivity near 0.02, the use of two coatings offers only a slight improvement in the glazing thermal performance [17]. Furthermore, Park et al. [110] compared the effects of low-E coating placement on the  $U$ -value of hybrid vacuum glazing, and the results indicated that the low-E coating placed within the cavity outperformed that within the insulating gap, with a 68.7% reduction.

To maintain a low  $U$ -value of vacuum glazing, the sealant is equally crucial [131]. Kim and Jeon [132] conducted a method consisting of melting and sealing with hydrogen mixed gas and carried out a sensitivity analysis of the process parameters. According to

**Table 12**  
Central and total  $U$ -values of different composited vacuum glazing.

Type	Ref.	Research method	$U$ -value ( $W \cdot m^{-2} \cdot K^{-1}$ )		Notes
			Central	Total	
Hybrid-vacuum glazing	Park et al. [110]	Experiment	1.37	—	Low-E within insulation gap
	Fang et al. [118]	FEM	0.43	—	Low-E within vacuum gap
			0.33	—	Vacuum facing warm side
Triple-vacuum glazing	Baek and Kim [119]	WINDOW	0.49	—	Vacuum facing cold side
			0.26	—	CO <sub>2</sub> gap (15 mm)
	Saim Memon [96]	FEM	0.28	0.94	Vacuum pressure of 0.001 Pa
	Fang et al. [111]	FEM	0.57	0.94	Emissivity = 0.18 (four coatings)
			0.25	0.67	Emissivity = 0.03 (four coatings)
EC-vacuum glazing	Fang and Eames [125]	FVM	0.51	1.06	Emissivity = 0.02 (two coatings)
PV-vacuum glazing	Huang et al. [97]	COMSOL	0.84	—	Optimized using aerogel
			0.23		

**Table 13**  
 $U$ -values of vacuum glazing with different edge-seal widths and thermal conductivities [133] (Unit:  $W \cdot m^{-2} \cdot K^{-1}$ ).

Width (mm)	Sealant thermal conductivity ( $W \cdot m^{-1} \cdot K^{-1}$ )				
	10.00	6.00	1.00	0.10	0.05
6	0.898	0.897	0.886	0.825	0.782
8	0.934	0.934	0.921	0.862	0.819
10	0.966	0.964	0.959	0.897	0.854
12.5	1.011	1.009	0.997	0.936	0.893

Miao et al. [36], the thermal performance of vacuum glazing is affected by the sealing temperature. When the sealing temperature is below 400 °C, the  $U$ -value is 1.6  $W \cdot m^{-2} \cdot K^{-1}$ , and it decreases to 0.92  $W \cdot m^{-2} \cdot K^{-1}$  at 500 °C. With respect to the edge seal width, as it decreases from 10 to 3 mm, the central and total  $U$ -values of vacuum glazing with dimensions of 300 mm (length)  $\times$  300 mm (width) are reduced by 11.0% and 13.3%, respectively [104]. The  $U$ -values of large-dimensional vacuum glazing with dimensions of 500 mm (length)  $\times$  500 mm (width) and 1000 mm (length)  $\times$  1000 mm (width) decreased by 21.1% and 20.3%, respectively [128]. Therefore, vacuum glazing with a narrower seal edge results in a lower heat transfer coefficient. In addition to the edge seal width, researchers have investigated the  $U$ -values of vacuum glazing with different edge seal widths and materials [37,51], and the results are listed in Table 13. Notably, the  $U$ -value of vacuum glazing with the lowest sealant thermal conductivity and width is 0.782  $W \cdot m^{-2} \cdot K^{-1}$ .

## 6. Energy-savings potential analysis

In terms of the thermal performance of vacuum glazing under standard winter conditions, a lower heat transfer coefficient signifies better insulation and a greater reduction in heat loss. Nonetheless, vacuum glazing encounters varying environmental conditions in practical applications. Significant disparities may arise when the energy-savings potential of vacuum glazing is investigated solely in terms of how well it performs under standard conditions rather than considering its true impact. Therefore, researchers have conducted annual dynamic energy consumption simulations to investigate the energy-savings potential of various types of vacuum glazing across diverse climates, as listed in Table 14.

In central Edinburgh, UK, the use of traditional vacuum glazing with a  $U$ -value of 1.4  $W \cdot m^{-2} \cdot K^{-1}$  can lead to annual savings in heating expenses of over 500 USD [134]. In Dublin, vacuum glazing decreases heat loss by 53% compared with a glazing unit with a  $U$ -value of 2.9  $W \cdot m^{-2} \cdot K^{-1}$  [135]. Cho and Kim [136] reported that the energy consumption of vacuum glazing decreased as the pillar interval increased, reaching a maximum savings of 2.46% compared with that of double glazing in an office building located in

**Table 14**  
Summary of energy-saving potential of vacuum glazing.

Type	Ref.	U-value (W·m <sup>-2</sup> ·K <sup>-1</sup> )	Location	Building			Energy efficiency performance	
				Type	Dimension (length (m) × width (m) × height (m))	Orientation		WWR
Double vacuum	McSporrán [134]	1.4	Edinburgh, UK (26°N, 98°W)	Museum	—	—	—	The use of vacuum glazing can save over 500 USD per year on heating costs and 32 tonnes of CO <sub>2</sub> over the lifetime of the window
	Ghosh et al. [135]	1.4	Dublin, Ireland (53°N, 6.25°W)	Test cell	—	—	—	Vacuum glazing can decrease 53% heat loss compared to double-pane glazing
	Cho and Kim [136]	0.68–1.47	Inchon, Republic of Korea (37°N, 126°E)	Office	32.40 × 32.40 × 2.80	East, north, west, and south	60%	Compared to double glazing, the heating and cooling energy usage can be reduced by 2.46%
Multi- pane vacuum	Beak and Kim [137]	0.7	Seoul, Republic of Korea (38°N, 127°E)	Apartment	—	—	40%	Vacuum glazing decreased the annual energy usage from 3365.5 to 1308.8 kW·h, in comparison to double glazing
	Kim et al. [46]	0.51–0.56	Republic of Korea	Office	3.60 × 2.40 × 2.60	—	—	Hybrid vacuum glazing can decrease the total energy usage of residential buildings by 12% and office buildings by 2.7%
	Park et al. [110]	0.30–0.50	Daejeon, Republic of Korea (36°N, 127°E)	Residential	—	—	—	The indoor–outdoor surface temperature disparity is up to 35.1 and 23.1 °C for vacuum glazing and triple-pane glazing
	Baek and Kim [119]	0.26	Seoul, Republic of Korea (38°N, 127°E)	Residential	5.0 0 × 5.00 × 2.50	South	48%	The heating energy consumption in buildings with air, CO <sub>2</sub> , argon, and krypton gas was 643.47, 639.75, 637.50, and 634.20 kW·h
	McSporrán [134]	0.9	Japan (35°N, 139°E)	Residential	—	—	—	Compared to double-pane glazing, the hybrid vacuum glazing with a 12 mm argon gap can save more than 20% air conditioning costs
	Beak and Kim [137]	0.61–1.15	Inchon, Republic of Korea (37°N, 126°E)	Office	32.40 × 32.40 × 2.80	East, north, west, and south	60%	Triple vacuum glazing can reduce heating and cooling energy usage by 3.91%
Tinted- vacuum PV-vacuum	Aritra Ghosh [51]	1.10	London, UK (52°N, -0.1°E) Delhi, India (29°N, 77°E)	Test cell	0.37 × 0.22 × 0.26	—	—	Conventional vacuum glazing is the best choice in London, while tinted vacuum glazing performs better than vacuum and double-pane glazing in Delhi
	Tan et al. [45,112]	0.89	Harbin, China (46°N, 127°E) Beijing, China (40°N, 117°E) Changsha, China (28°N, 113°E) Guangzhou, China (23°N, 113°E) Kunming, China (25°N, 102°E)	Office	—	East, south, west, and north	—	The energy usage of PV-vacuum glazing can be reduced by 23–128 kW·h·m <sup>-2</sup> in Harbin, Beijing, Changsha, and Guangzhou
	Qiu and Yang [78] and Qiu et al. [138]	0.56	Harbin, China (46°N, 127°E) Beijing, China (40°N, 117°E) Wuhan, China (31°N, 114°E) Hong Kong, China (22°N, 114°E)	Office	2.30 × 3.00 × 2.50	South	66%	PV-vacuum glazing can save up to 43.4%, 66.0%, 48.8%, and 35.0% more energy than double glazing in Harbin, Beijing, Wuhan, and Hong Kong
	Huang et al. [139]	0.56	Harbin, China (46°N, 127°E) Beijing, China (40°N, 117°E) Wuhan, China (31°N, 114°E) Guangzhou, China (23°N, 113°E)	Office	—	South	—	The PV-vacuum glazing can decrease the net energy usage by 62.7, 65.1, 26.2, and 21.0 kW·h compared to double glazing
	Uddin et al. [140]	1.15	Hohhot, China (40°N, 111°E) Tianjin, China (39°N, 117°E) Hefei, China (32°N, 117°E) Kunming, China (25°N, 102°E) Xiamen, China (24°N, 118°E)	Office	5.45 × 4.65 × 3.30	South	17.1% 34.3% 51.4% 68.6%	Compared to the window with 17.1% WWR, the PV-vacuum glazing at 68.6% of WWR can save annual net energy consumption of 30.3%, 36.5%, 13.7%, 84.5%, and 45.1% in Hohhot, Tianjin, Hefei, Kunming, and Xiamen.

35

Inchon, Republic of Korea. In addition, Beak and Kim [137] examined the energy usage of a typical apartment building with vacuum glazing in Seoul, Republic of Korea. The results indicated that the total annual energy consumption was 3365.5, 2617.6, 2243.7, and 1308.8 kW·h with double, triple, quadruple, and vacuum glazing, respectively.

With respect to multipane vacuum glazing, Kim et al. [46] evaluated the impacts of hybrid vacuum glazing on office and residential energy consumption in Republic of Korea, as illustrated in Fig. 17. Compared with low-E glazing (LEG), hybrid vacuum glazing with a vacuum layer facing outside (IVG), single vacuum glazing (SVG), and hybrid vacuum glazing with a vacuum layer facing inside (OVG) can reduce heating energy consumption in office buildings by 11%, 15%, and 13%, respectively. Conversely, for IVG, SVG, and OVG, the increases in cooling energy consumption were approximately 2%, 6%, and 4%, respectively. In residential buildings, IVG, SVG, and OVG exhibited 10%, 30%, and 20% more cooling energy, respectively. However, heating energy usage with IVG, SVG, and OVG can be decreased by 17%, 24%, and 21%, respectively.

Baek and Kim [119] reported that the 10-day heating energy consumption values of buildings with hybrid vacuum glazing filled with CO<sub>2</sub>, air, argon, and Krypton gases were 643.47, 639.75, 637.50, and 634.20 kW·h, respectively. Park et al. [110] conducted experiments in Daejeon, Republic of Korea to evaluate the thermal performance of vacuum glazing and reported that the average edge surface temperature of vacuum glazing was 5.3 to 5.8 °C higher than that of triple-pane glazing, indicating superior thermal performance.

In addition to traditional double-pane and multilayer vacuum glazing, researchers have carried out studies on the energy performance of innovative tinted and PV vacuum glazing. Aritra Ghosh [51] reported that vacuum glazing provided 29.1% more net heat gain than double glazing, whereas tinted vacuum glazing provided 9% and 11% less net heat gain in both the on and off states, respectively. Vacuum glazing and tinted vacuum glazing are the best options for London and Delhi considering the overall climate, owing to their highest and lowest yearly net gains. Qiu and Yang [78] and Qiu et al. [138] reported that PV vacuum glazing can reduce energy usage by 35.0%–66.0%. Compared with conventional double-pane glazing, PV vacuum glazing can decrease net energy usage by 62.7, 65.1, 26.2, and 21.0 kW·h, respectively [139]. Uddin et al. [140] reported that increasing the window to wall ratio (WWR) from 17.1% to 68.6% with PV vacuum glazing can reduce annual net energy consumption by 30.3%, 36.5%, 13.7%, 84.5%, and 45.1% in Hohhot, Tianjin, Hefei, Kunming, and Xiamen, respectively. Furthermore, PV vacuum glazing can achieve zero energy consumption during 67% of operating hours by optimizing the coating emissivity and other configurations in Changsha [45].

On the basis of the above analysis, vacuum glazing in various structures clearly offers distinct energy-savings potential across diverse buildings and climate regions. For severely cold and cold climates, triple vacuum glazing has the highest energy-savings potential because it has the lowest heat transfer coefficient, which minimizes heat loss and reduces building energy consumption. In the hot summer and cold winter zones, vacuum glazing with solar radiation modulation capability is more suitable, as it introduces solar heat gain in winter and reduces unwanted heat in summer. Furthermore, in regions abundant in solar radiation resources, PV vacuum glazing exhibits superior performance because it not only reduces heat loss but also efficiently harnesses solar radiation to generate clean electricity. Therefore, PV vacuum glazing significantly enhances building energy efficiency by addressing both energy conservation and production. From an architectural orientation perspective, there is no significant difference in the applicability of traditional double-pane vacuum glazing and multicavity vacuum glazing across different orientations. However, tinted and PV vacuum glazing are more suitable for south-facing orientations (in the Northern Hemisphere), where solar radiation resources are relatively abundant.

### 7. Conclusions

This paper presents a comprehensive review of recent studies on the thermal performance of vacuum glazing, covering its materials, fabrication approaches, composite structures, research methods, and energy-savings potential. The evolution of vacuum glazing was outlined, and commonly used fabrication techniques were compared, with a focus on sealing technologies and support pillar arrangements. Various composite vacuum glazing structures were subsequently introduced, and their advantages and disadvantages were compared. This review also discusses different methods for analyzing the thermal performance and composite structure of vacuum glazing, including analytical, numerical, and experimental methods. Furthermore, the *U*-values of vacuum glazing with typical structures were summarized, the influences of different parameters on the *U*-values were elaborated in detail, and the energy-savings potential of vacuum glazing in various scenarios was outlined. The systematic literature review identified research gaps, challenges, and future developments in vacuum glazing, and the primary findings are as follows:

- The modified PO method has emerged as the most suitable manufacturing approach; it can effectively overcome the drawbacks of both the glass powder sealing method, which is prone to high-temperature degradation, and the VC method, which often suffers from insufficient outgassing.

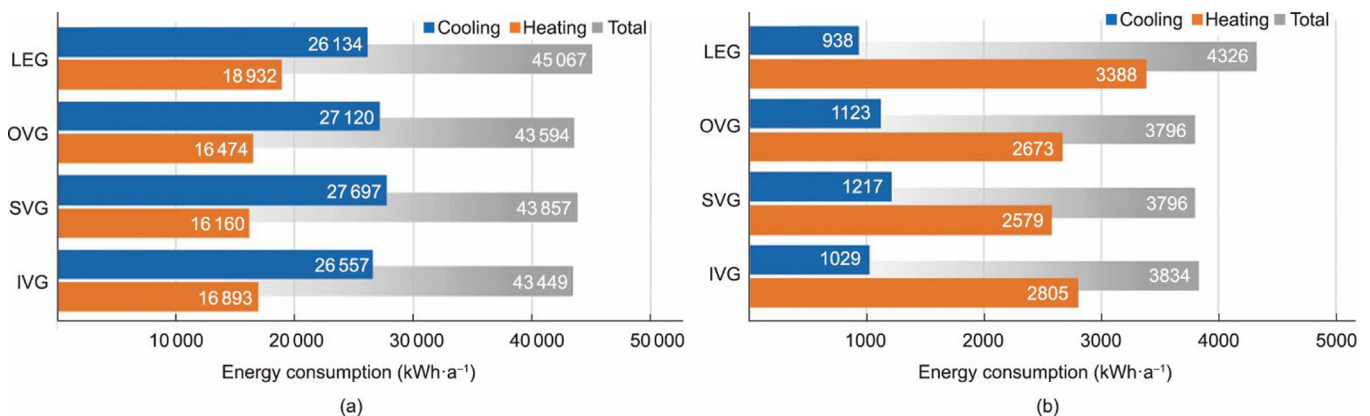


Fig. 17. Energy consumption with different glazing units in (a) office and (b) residential buildings [46].

- Vacuum glazing integrated with other technologies can fulfill multiple functions. Triple vacuum glazing yields a  $U$ -value of  $0.2 \text{ W}\cdot\text{m}^{-2}\cdot\text{K}^{-1}$ , tinted vacuum glazing can simultaneously achieve excellent insulation and dynamic solar modulation, and PV vacuum glazing can achieve net-zero energy consumption for half of the working time of the year.
- The vacuum level and low-E coating emissivity significantly affect the thermal performance of vacuum glazing. The energy-savings potential of vacuum glazing and its composite structures is not only dependent on their performance but also closely linked to factors such as building types, dimensions, orientations, climates, and other building operational factors.
- Triple vacuum glazing performs effectively in severely cold and cold climates; tinted vacuum glazing is suitable for regions with significant seasonal variations in heating and cooling demands; and PV vacuum glazing has exceptional energy efficiency performance in regions and orientations with abundant solar radiation.

In addition to current research efforts, further studies should be conducted on the stability and industrialization of vacuum glazing with aerogel support pillar arrays. Additionally, it is crucial to determine the appropriate control strategy for tinted vacuum glazing to maximize its solar modulation benefits. The aging process and effective service life of vacuum glazing and its composite structures should also be considered when evaluating their energy-savings potentials.

#### CRedit authorship contribution statement

**Jinqing Peng:** Writing – review & editing, Supervision, Funding acquisition. **Yutong Tan:** Writing – review & editing, Writing – original draft, Visualization, Funding acquisition, Conceptualization. **Yueping Fang:** Writing – review & editing. **Hongxing Yang:** Writing – review & editing. **Aotian Song:** Resources. **Charlie Curcija:** Writing – review & editing. **Stephen Selkowitz:** Writing – review & editing.

#### Declaration of competing interest

The authors declare that they have no known competing financial interests or personal relationships that could have appeared to influence the work reported in this paper.

#### Acknowledgments

This study was supported by the National Key R&D Program of China (2023YFC3806202), the National Natural Science Foundation of China (52308093), the Natural Science Foundation of Hunan Province (2023JJ40154), the Science and Technology Innovation Leading Talent Program of Hunan Province (2023RC1042), the Natural Science Foundation of Changsha (kq2208032), and the China Postdoctoral Science Foundation (2023M741132 and 2024T170263).

#### References

- [1] Ke Y, Zhou C, Zhou Y, Wang S, Chan SH, Long Y. Emerging thermal-responsive materials and integrated techniques targeting the energy-efficient smart window application. *Adv Funct Mater* 2018;28(22):1800113.
- [2] Cuce E, Riffat SB. A state-of-the-art review on innovative glazing technologies. *Renew Sustain Energy Rev* 2015;41:695–714.
- [3] Abd-Alhamid F, Kent M, Calautit J, Wu Y. Evaluating the impact of viewing location on view perception using a virtual environment. *Build Environ* 2020;180:106392.
- [4] Pérez-Lombard L, Ortiz J, Pout C. A review on buildings energy consumption information. *Energy Build* 2008;40(3):394–8.

- [5] Abraham E, Cherpak V, Senyuk B, ten Hove JB, Lee T, Liu Q, et al. Highly transparent silanized cellulose aerogels for boosting energy efficiency of glazing in buildings. *Nat Energy* 2023;8(4):381–96.
- [6] Sorooshnia E, Rashidi M, Rahnamayiezekavat P, Mahmoudkelayeh S, Pourvaziri M, Kamranfar S, et al. A novel approach for optimized design of low-E windows and visual comfort for residential spaces. *Energy Build Environ* 2025;6(1):27–42.
- [7] Somasundaram S, Chong A, Wei Z, Thangavelu SR. Energy saving potential of low-e coating based retrofit double glazing for tropical climate. *Energy Build* 2020;206:109570.
- [8] Urbikain MK. Energy efficient solutions for retrofitting a residential multi-storey building with vacuum insulation panels and low-E windows in two European climates. *J Clean Prod* 2020;269:121459.
- [9] Tiwari R, Kim J. Multi-cell, triple pane, vacuum insulated glazing. *Sol Energy* 2022;245:340–52.
- [10] Eames PC. Vacuum glazing: current performance and future prospects. *Vacuum* 2008;82(7):717–22.
- [11] Bhuiya MMH, Anderson AM, Carroll MK, Bruno BA, Ventrella JL, Silberman B, et al. Preparation of monolithic silica aerogel for fenestration applications: scaling up, reducing cycle time, and improving performance. *Ind Eng Chem Res* 2016;55(25):6971–81.
- [12] Wei G, Wang L, Xu C, Du X, Yang Y. Thermal conductivity investigations of granular and powdered silica aerogels at different temperatures and pressures. *Energy Build* 2016;118:226–31.
- [13] Yunos L, Jane ML, Murphy PJ, Zuber K. Frequency selective surface on low emissivity windows as a means of improving telecommunication signal transmission: a review. *J Build Eng* 2023;70:106416.
- [14] Pilkington. Understanding the government's data on  $U$  values. Indicative  $U$  values for windows with wood or PVC- $U$  frames [Internet]. Tokyo: Pilkington; [Cited 2025 Aug 10]. Available from: <https://www.pilkington.com/~/media/Pilkington/Site%20Content/UK/Reference/TableofDefaultUValues.pdf>.
- [15] Lolli N, Andresen I. Aerogel vs. argon insulation in windows: a greenhouse gas emissions analysis. *Build Environ* 2016;101:64–76.
- [16] Fang Y, Hyde TJ, Arya F, Heewitt N. A novel building component hybrid vacuum glazing a modelling and experimental validation. *ASHRAE Trans* 2013;119:430–40.
- [17] Fang Y, Eames PC, Norton B, Hyde TJ, Zhao J, Wang J, et al. Low emittance coatings and the thermal performance of vacuum glazing. *Sol Energy* 2007;81(1):8–12.
- [18] Ihara T, Grynning S, Gao T, Gustavsen A, Jelle BP. Impact of convection on thermal performance of aerogel granulate glazing systems. *Energy Build* 2015;88:165–73.
- [19] Liu Y, Chen Y, Lu L, Peng J, Zheng D, Lu B. Optical path model and energy performance optimization of aerogel glazing system filled with aerogel granules. *Appl Energy* 2023;334:120623.
- [20] Zoller A, assignee. Hollow pane of glass. German patent DE 387655C. 1924.
- [21] Cuce E. Development of innovative window and fabric technologies for low-carbon buildings [dissertation]. Nottingham: University of Nottingham; 2014.
- [22] Benson DTC, Jorgenson J. Laser sealed evacuated window glazings. In: Proceedings of the 28th Annual SPIE. International Technical Symposium on. Optics and Electro-Optics; 1984 Aug 19–24; San Diego, CA, USA. Washington: US Department of Energy; 1985.
- [23] Robinson SJ, Collins RE. Evacuated windows-theory and practices. In: Proceedings of the ISES Solar World Congress; 1989 Sep 4–8; Kobe, Japan. Boulder: American Solar Energy Society; 1989.
- [24] Collins RE, Simko TM. Current status of the science and technology of vacuum glazing. *Sol Energy* 1998;62(3):189–213.
- [25] Pilkington. Pilkington Spacia brochure. Tokyo: Pilkington; 2018.
- [26] BGriffiths PW, di Leo M, Cartwright P, Eames PC, Yianoulis P, Leftheriotis G, et al. Fabrication of evacuated glazing at low temperature. *Sol Energy* 1998;63(4):243–9.
- [27] Hyde TGP, Eames P, Norton B. Development of a novel low temperature edge seal for evacuated glazing. In Proceedings of the World Renewable Energy Congress VI; 2000 Jul 1–7; Brighton, UK. Amsterdam: Elsevier; 2000. p. 271–4.
- [28] Curcija DC, Hart RG. Modeling thermal performance of VIG: WINDOW and THERM software tools. In: Proceedings of the 1st China (Qingdao) International Glass & Equipment Technology Seminar; 2018 Aug; Qingdao, China. Berkeley: Lawrence Berkeley National Laboratory; 2018.
- [29] Fang Y, Hyde TJ, Arya F, Hewitt N, Eames PC, Norton B, et al. Indium alloy-sealed vacuum glazing development and context. *Renew Sustain Energy Rev* 2014;37:480–501.
- [30] Cuce E, Cuce PM. Vacuum glazing for highly insulating windows: recent developments and future prospects. *Renew Sustain Energy Rev* 2016;54:1345–57.
- [31] Ali H, Hayat N, Farukh F, Imran S, Kamran M, Ali H. Key design features of multi-vacuum glazing for windows: a review. *Therm Sci* 2017;21(6 Pt B):2673–87.
- [32] Uddin MM, Jie J, Wang C, Zhang C, Ke W. A review on photovoltaic combined vacuum glazing: recent advancement and prospects. *Energy Build* 2023;286:112939.
- [33] Garrison JCR, Collins RE. Manufacture and cost of vacuum glazing. *Sol Energy* 1995;55(3):151–61.
- [34] Zhao JF, Eames PC, Hyde TJ, Fang Y, Wang J. A modified pump-out technique used for fabrication of low temperature metal sealed vacuum glazing. *Sol Energy* 2007;81(9):1072–7.

- [35] Griffiths PW, Eames PC, Hyde TJ, Fang Y, Norton B. Experimental characterization and detailed performance prediction of a vacuum glazing system fabricated with a low temperature metal edge seal, using a validated computer model. *J Sol Energy Eng* 2006;128(2):199–203.
- [36] Miao H, Mei Q, Zhang J, Yuan J, Shan X. The influence of sealing temperature on the thermal and light properties of low-E coating vacuum glazing. *J Ceram Soc Jpn* 2016;124(4):469–74.
- [37] Memon S. Experimental measurement of hermetic edge seal's thermal conductivity for the thermal transmittance prediction of triple vacuum glazing. *Case Stud Therm Eng* 2017;10:169–78.
- [38] Falbel G, inventor; Energy Science Inc., assignee. Evacuated dual glazing system. United States patent US 3990201A. 1976.
- [39] Collins RE, Fischer-Cripps AC. Design of support pillar arrays in flat evacuated windows. *Aust J Phys* 1991;44(5):545.
- [40] Collins RAO, Misonou M. Vacuum glazing: design options and performance capability. In: Proceedings of the Glass Building's Conference 1999; 1999 Jun 13–16; Tampere, Finland. Helsinki: National Library of Finland; 1999.
- [41] Henshall P, Eames P, Arya F, Hyde T, Moss R, Shire S. Constant temperature induced stresses in evacuated enclosures for high performance flat plate solar thermal collectors. *Sol Energy* 2016;127:250–61.
- [42] Fischer-Cripps AC. Introduction to contact mechanics. Berlin: Springer; 2007.
- [43] Chen B, Lv H, Liao J, Dong S, Cheng C, Lv Q, et al. Thermal insulation performance of an advanced photovoltaic vacuum glazing: a numerical investigation and simulation. *J Renew Sustain Energy* 2019;11(1):015101.
- [44] Fang Y, Eames PC, Norton B. Effect of glass thickness on the thermal performance of evacuated glazing. *Sol Energy* 2007;81(3):395–404.
- [45] Tan Y, Peng J, Luo Y, Li H, Wang M, Zhang F, et al. Daylight–electrical–thermal coupling model for real-time zero-energy potential analysis of vacuum-photovoltaic glazing. *Renew Energy* 2023;205:1040–56.
- [46] Kim SC, Yoon JH, Lee RD. Energy performance assessment of a 2nd-generation vacuum double glazing depending on vacuum layer position and building type in Republic of Korea. *Energies* 2017;10(8):1240.
- [47] Bao M, Liu X, Yang J, Bao Y. Novel hybrid vacuum/triple glazing units with pressure equalisation design. *Constr Build Mater* 2014;73:645–51.
- [48] Manz H, Brunner S, Wullschlegel L. Triple vacuum glazing: heat transfer and basic mechanical design constraints. *Sol Energy* 2006;80(12):1632–42.
- [49] Ghosh A, Norton B, Duffy A. Measured thermal performance of a combined suspended particle switchable device evacuated glazing. *Appl Energy* 2016;169:469–80.
- [50] Mesloub A, Ghosh A, Touahmia M, Albaqawy GA, Alsolami BM, Ahriz A. Assessment of the overall energy performance of an SPD smart window in a hot desert climate. *Energy* 2022;252:124073.
- [51] Ghosh A. Investigation of vacuum-integrated switchable polymer dispersed liquid crystal glazing for smart window application for less energy-hungry building. *Energy* 2023;265:126396.
- [52] Han C, Lee J, An C, Oh S. A liquid crystal smart window for energy saving and harvesting. *Appl Mater Today* 2023;35:101923.
- [53] Papaefthimiou S, Leftheriotis G, Yianoulis P, Hyde TJ, Eames PC, Fang Y, et al. Development of electrochromic evacuated advanced glazing. *Energy Build* 2006;38(12):1455–67.
- [54] Villa DL, Hahn NT, Grey JK, Pavich F. Futures for electrochromic windows on high performance houses in arid, cold climates. *Energy Build* 2024;315:114293.
- [55] Fischer UHT, Rogab H, Rottmann M, Kraft A, Heckner K. Heat transport and thermal expansion of electrochromic glazing systems with voltage controlled transmission due to solar irradiation. In: Proceedings of the Fifteenth Symposium on Thermophysical Properties; 2003 Jun 22–27; Boulder, CO, USA. Berlin: Springer; 2003.
- [56] Fang YEP, Eames PC. Thermal performance of an electrochromic vacuum glazing. *Energy Conserv Manag* 2006;47(20):3602–10.
- [57] Fang Y, Eames PC, Norton B, Hyde T, Huang Y, Hewitt N. The thermal performance of an electrochromic vacuum glazing with selected low-emittance coatings. *Thin Solid Films* 2008;516(6):1074–81.
- [58] Ghosh A, Sundaram S, Mallick TK. Colour properties and glazing factors evaluation of multicrystalline based semi-transparent Photovoltaic-vacuum glazing for BIPV application. *Renew Energy* 2019;131:730–6.
- [59] Lyu YL, Liu WJ, Su H, Wu X. Numerical analysis on the advantages of evacuated gap insulation of vacuum-water flow window in building energy saving under various climates. *Energy* 2019;175:353–64.
- [60] Lyu Y, Zheng S, Zhuo K, Su H, Li J, Liu C. Experimental and numerical performance investigation of a water-flow window with vacuum-glazing insulation. *Sol Energy* 2022;233:259–70.
- [61] Schultz JM, Jensen KI. Evacuated aerogel glazings. *Vacuum* 2008;82(7):723–79.
- [62] Zhang X, Liu Z, Wang P, Li B. Performance evaluation of a novel rotatable dynamic window integrated with a phase change material and a vacuum layer. *Energy Convers Manage* 2022;272:116333.
- [63] Ahmed M, Radwan A, Serageldin A, Memon S, Katsura T, Nagano K. Thermal analysis of a new sliding smart window integrated with vacuum insulation, photovoltaic and phase change material. *Sustainability* 2020;12(19):7846.
- [64] NSG Group. NSG Group official social media [Internet]. Tokyo: Nippon Sheet Glass Co., Ltd.; [cited 2024 Dec 6]. Available from: <https://www.nsg.com/Media>.
- [65] Panasonic Group. Panasonic newsroom global [Internet]. Osaka: Panasonic Group; [cited 2024 Dec 6]. Available from: <https://news.panasonic.com/global/>.
- [66] FINEO. Vacuum glazing [Internet]. Neckar: FINEO; [cited 2024 Dec 6]. Available from: <https://www.fineoglass.eu/>.
- [67] Vitro Architectural Glass. VacuMax™ Vacuum insulating glass [Internet]. Cheswick: Vitro Architectural Glass; [cited 2024 Dec 6]. Available from: <https://www.vitroglazings.com/products/specialty-glass-applications/vacumax-vacuum-insulating-glass/>.
- [68] Luxwall.com [Internet]. Ypsilanti: LuxWall; [cited 2024 Dec 6]. Available from: <https://www.luxwall.com/>.
- [69] Synergy. Synergy energy saving glass [Internet]. Tianjin: Synergy Energy Saving Glass (Tianjin) Co., Ltd.; [cited 2024 Dec 6]. Available from: <http://en.xinliji-vg.com/>.
- [70] LandVac. Vacuum Glass [Internet]. Luoyang: LandVac; [cited 2024 Dec 6]. Available from: <https://www.vacuum-glass.net/>.
- [71] ICESUN VACUUM GLASS LTD. Vacuum glass [Internet]. Montague: ICESUN VACUUM GLASS LTD.; [cited 2024 Dec 6]. Available from: <https://vacuumglass.ca/>.
- [72] LEADUS. Product [Internet]. Shenzhen: Shenzhen Leadus Technology Industry Co., Ltd.; [cited 2024 Dec 6]. Available from: <https://www.leadustech.com/>.
- [73] Sun Y, Wu Y, Wilson R. A review of thermal and optical characterization of complex window systems and their building performance prediction. *Appl Energy* 2018;222:729–47.
- [74] Onatayo D, Aggarwal R, Srinivasan RS, Shah B. A data-driven approach to thermal transmittance (*U*-factor) calculation of double-glazed windows with or without inert gases between the panes. *Energy Build* 2024;305:113907.
- [75] Chmurny I. Thermal transmittance around edge of vacuum glazing. *IOP Conf Series Mater Sci Eng* 2019;603(2):022059.
- [76] Ghosh A, Sarmah N, Sundaram S, Mallick TK. Numerical studies of thermal comfort for semi-transparent building integrated photovoltaic (BIPV)-vacuum glazing system. *Sol Energy* 2019;190:608–16.
- [77] Curcija C VS, Hart R, Jonsson J, Mitchell R. WINDOW technical documentation. Report. Berkeley: University of California Berkeley; 2018.
- [78] Qiu C, Yang H. Dynamic coupling of a heat transfer model and whole building simulation for a novel cadmium telluride-based vacuum photovoltaic glazing. *Energy* 2022;250:12375.
- [79] Khalifa AMR, Marshall RH. Validation of heat transfer coefficient on interior building surfaces using a real-sized indoor test cell. *Int J Heat Mass Transf* 1990;33(10):2219–36.
- [80] ASTM C1363-24. Standard test method for thermal performance of building materials and envelop assemblies by means of a hot box apparatus. ASTM standard. West Conshohocken: ASTM International; 2024.
- [81] ISO 10077-1:2006. Thermal performance of windows, doors, and shutters—calculation of thermal transmittance—part 1: simplified method. ISO standard. Brussels: International Organization for Standardization (ISO); 2006.
- [82] KS F 2278—2014. Standard test method for thermal resistance for windows and doors. Republic of Korean standard. Chungcheongbuk-do: Republic of Korean Agency for Technology and Standards; 2014.
- [83] JGJ/T 151—2008. Calculation specification for thermal performance of windows, doors, and glass curtain-walls. Chinese standard. Beijing: Ministry of Housing and Urban-Rural Development of the People's Republic of China; 2016. Chinese.
- [84] GB/T 22476—2008. Calculation and determination of steady-state *U*-values (thermal transmittance) of multiple glazing. Chinese standard. Beijing: National Standardization Administration of the People's Republic of China; 2008. Chinese.
- [85] Cooper MG, Mikic BB, Yovanovich MM. Thermal conductance. *Int J Heat Mass Transf* 1969;12(3):279–300.
- [86] Zhu W, Zhang S, Shin S, Gorti S, Shah B, Joshi P, et al. Effects of pillar design on the thermal performance of vacuum-insulated glazing. *Constr Build Mater* 2022;316:125724.
- [87] Xu L. Low temperature vacuum technology. Beijing: China Machine Press; 2008. Chinese.
- [88] Da DA. Vacuum design manual. 3rd ed. Beijing: National Defense Industry Press; 2004. Chinese.
- [89] Simko TM, Collins RE, Beck FA, Arasteh DK. Edge conduction in vacuum glazing. In: Proceedings of the Thermal Performance of Exterior Envelopes of Buildings VI Conference; 1995 Dec 4–8; Clearwater, FL, USA. Atlanta: American Society of Heating, Refrigerating and Air-Conditioning Engineers, Inc; 1995.
- [90] Simkoa TM, Fischer-Cripps AC, Collins RE. Heat transfer processes and stresses in vacuum glazing. *Sol Energy* 1998;63(1):1–21.
- [91] Fang Y, Hyde TJ, Hewitt N. Predicted thermal performance of triple vacuum glazing. *Sol Energy* 2010;84(12):2132–9.
- [92] ASTM E1423-21. Standard practice for determining steady state thermal transmittance of fenestration systems. ASTM standard. West Conshohocken: ASTM International; 2021.
- [93] Wullschlegel L, Manz H, Ghazi WK. Finite element analysis of temperature-induced deflection of vacuum glazing. *Constr Build Mater* 2009;23(3):1378–88.
- [94] Hu D, Li Y, Liu C, Li Y. Analysis for the heat transfer of fully tempered vacuum glazing based on the thermal resistance model and finite element model. *Adv Mech Eng* 2018;10(9):94.

- [95] Fang Y, Eames PC, Norton B, Hyde TJ. Experimental validation of a numerical model for heat transfer in vacuum glazing. *Sol Energy* 2006;80(5):564–77.
- [96] Memon S, Farukh F, Kandan K. Effect of cavity vacuum pressure diminution on thermal performance of triple vacuum glazing. *Appl Sci* 2018;8(9):1705.
- [97] Huang J, Chen X, Peng J, Yang H. Modelling analyses of the thermal property and heat transfer performance of a novel composite PV vacuum glazing. *Renew Energy* 2021;163:1238–52.
- [98] Shi Y, Xi X, Zhang Y, Xu H, Zhang J, Zhang R. Prediction and analysis of the thermal performance of composite vacuum glazing. *Energies* 2021;14(18):5769.
- [99] Memon S, Farukh F, Eames PC, Silberschmidt VV. A new low-temperature hermetic composite edge seal for the fabrication of triple vacuum glazing. *Vacuum* 2015;120:73–82.
- [100] Wang J, Eames PC, Zhao JF, Hyde T, Fang Y. Stresses in vacuum glazing fabricated at low temperature. *Sol Energy Mater Sol Cells* 2007;91(4):290–303.
- [101] Fang Y, Hyde TJ, Arya F, Hewitt N. Modelling and experimental validation for the thermal performance of a hybrid vacuum glazing. In: *Proceedings of the Energy & Materials Research Conference (EMR2012)*; 2012 Jun 20–22; Malaga, Spain. Norristown: Formatek Research Center; 2012.
- [102] Katsura T, Memon S, Radwan A, Nakamura M, Nagano K. Thermal performance analysis of a new structured-core translucent vacuum insulation panel in comparison to vacuum glazing: experimental and theoretically validated analyses. *Sol Energy* 2020;199:326–46.
- [103] Fang Y, Arya F. Evacuated glazing with tempered glass. *Sol Energy* 2019;183:240–7.
- [104] Memon S, Fang Y, Eames PC. The influence of low-temperature surface induction on evacuation, pump-out hole sealing and thermal performance of composite edge-sealed vacuum insulated glazing. *Renew Energy* 2019;135:450–64.
- [105] Rao SS. *The finite element method in Engineering*. 4th ed. Amsterdam: Elsevier Inc.; 2005.
- [106] Fang Y, Hyde T, Hewitt N, Eames PC, Norton B. Comparison of vacuum glazing thermal performance predicted using two- and three-dimensional models and their experimental validation. *Sol Energy Mater Sol Cells* 2009;93(9):1492–8.
- [107] Kumar S. Investigation of 3-D heat transfer effects in fenestration products [dissertation]. Amherst: University of Massachusetts Amherst; 2010.
- [108] Ghosh A, Ghosh S, Neogi S. Performance evaluation of a guarded hot box  $U$ -value measurement facility under different software based temperature control strategies. *Energy Procedia* 2014;54:448–54.
- [109] Chmurny I, Szabo D. Thermal irregularities in vacuum glazing. *IOP Conf Ser Mater Sci Eng* 2019;471:062012.
- [110] Park J, Oh M, Lee C. Thermal performance optimization and experimental evaluation of vacuum-glazed windows manufactured via the in-vacuum method. *Energies* 2019;12(19):3634.
- [111] Fang Y, Hyde TJ, Arya F, Hewitt N, Wang R, Dai Y. Enhancing the thermal performance of triple vacuum glazing with low-emittance coatings. *Energy Build* 2015;97:186–95.
- [112] Tan Y, Peng J, Luo Y, Luo Z, Curcija C, Fang Y. Numerical heat transfer modeling and climate adaptation analysis of vacuum-photovoltaic glazing. *Appl Energy* 2022;312:118747.
- [113] Fang Y, Eames PC, Hyde TJ, Norton B. Complex multimaterial insulating frames for windows with evacuated glazing. *Sol Energy* 2005;79(3):245–61.
- [114] Ng N, Collins RE, So L. Thermal conductance measurement on vacuum glazing. *Int J Heat Mass Transf* 2006;49(25–26):4877–85.
- [115] Ng N, Collins RE, So L. Characterization of the thermal insulating properties of vacuum glazing. *Mater Sci Eng B* 2007;138(2):128–34.
- [116] Qiu C, Yang H, Zhang W. Investigation on the energy performance of a novel semi-transparent BIPV system integrated with vacuum glazing. *Build Simul* 2019;12(1):29–39.
- [117] Zhang C, Ji J, Wang C, Ke W, Xie H, Yu B. Experimental and numerical studies on the thermal and electrical performance of a CdTe ventilated window integrated with vacuum glazing. *Energy* 2022;244:123128.
- [118] Fang Y, Memon S, Peng J, Tyrer M, Ming T. Solar thermal performance of two innovative configurations of air-vacuum layered triple glazed windows. *Renew Energy* 2020;150:167–75.
- [119] Baek S, Kim S. Optimum design and energy performance of hybrid triple glazing system with vacuum and carbon dioxide filled gap. *Sustainability* 2019;11(19):5543.
- [120] Nundy S, Ghosh A. Thermal and visual comfort analysis of adaptive vacuum integrated switchable suspended particle device window for temperate climate. *Renew Energy* 2020;156:1361–72.
- [121] Fang Y, Hyde T, Hewitt N, Eames PC, Norton B. Thermal performance analysis of an electrochromic vacuum glazing with low emittance coatings. *Sol Energy* 2010;84(4):516–25.
- [122] Jarimi H, Lv Q, Ramadan O, Zhang S, Riffat S. Design, mathematical modelling and experimental investigation of vacuum insulated semi-transparent thin-film photovoltaic (PV) glazing. *J Build Eng* 2020;31:101430.
- [123] Ghosh A, Sundaram S, Mallick TK. Investigation of thermal and electrical performances of a combined semi-transparent PV-vacuum glazing. *Appl Energy* 2018;228:1591–600.
- [124] Radwan A, Katsura T, Memon S, Serageldin AA, Nakamura M, Nagano K. Thermal and electrical performances of semi-transparent photovoltaic glazing integrated with translucent vacuum insulation panel and vacuum glazing. *Energy Convers Manage* 2020;215:112920.
- [125] Fang Y, Eames P. The effect of glass coating emittance and frame rebate on heat transfer through vacuum and electrochromic vacuum glazed windows. *Sol Energy Mater Sol Cells* 2006;90(16):2683–95.
- [126] Ghosh A, Norton B, Duffy A. Effect of atmospheric transmittance on performance of adaptive SPD-vacuum switchable glazing. *Sol Energy Mater Sol Cells* 2017;161:424–31.
- [127] Qiu C, Yang H. Daylighting and overall energy performance of a novel semi-transparent photovoltaic vacuum glazing in different climate zones. *Appl Energy* 2020;276:115414.
- [128] Zhu Q, Wu W, Yang Y, Han Z, Bao Y. Finite element analysis of heat transfer performance of vacuum glazing with low-emittance coatings by using ANSYS. *Energy Build* 2020;206:109584.
- [129] Cuce E, Riffat SB. Aerogel-assisted support pillars for thermal performance enhancement of vacuum glazing: a CFD research for a commercial product. *Arab J Sci Eng* 2015;40(8):2233–8.
- [130] Swimm K, Weinläder H, Ebert HP. Influence of spacer systems on heat transfer in evacuated glazing. *Int J Thermophys* 2009;30(3):934–48.
- [131] Kim JK, Kim YS, Jeon ES. Optimization of glass edge sealing process using microwaves for fabrication of vacuum glazing. *Appl Sci* 2019;9(5):874.
- [132] Kim Y, Jeon E. Sensitivity analysis of edge sealing process parameters of vacuum glazing panel. *Mol Cryst Liq Cryst* 2013;585(1):15–24.
- [133] Zhu W, Shah B, Gorti S, Bhandari M, Sabau AS, Shin S. Effects of edge-seal design on the mechanical and thermal performance of vacuum-insulated glazing. *Build Environ* 2022;224:109572.
- [134] McSparran N. Properties and performance of vacuum insulated glazing. *J Green Build* 2014;9(1):60–74.
- [135] Ghosh A, Norton B, Duffy A. Measured thermal & daylight performance of an evacuated glazing using an outdoor test cell. *Appl Energy* 2016;177:196–203.
- [136] Cho S, Kim SH. Analysis of the performance of vacuum glazing in office buildings in Republic of Korea: simulation and experimental studies. *Sustainability* 2017;9(6):936.
- [137] Baek S, Kim S. Potential effects of vacuum insulating glazing application for reducing greenhouse gas emission (GHGE) from apartment buildings in the Republic of Korean capital region. *Energies* 2020;13(11):2828.
- [138] Qiu C, Yang H, Sun H. Investigation on the thermal performance of a novel vacuum PV glazing in different climates. *Energy Procedia* 2019;158:706–11.
- [139] Huang J, Wang Q, Chen X, Xu S, Yang H. Experimental investigation and annual overall performance comparison of different photovoltaic vacuum glazings. *Sustain Cities Soc* 2021;75:103282.
- [140] Uddin MM, Wang C, Zhang C, Ji J. Investigating the energy-saving performance of a CdTe-based semi-transparent photovoltaic combined hybrid vacuum glazing window system. *Energy* 2022;253:124019.